Salinomycin Inhibits Influenza Virus Infection by Disrupting Endosomal Acidification and Viral Matrix Protein 2 Function

Running title: *In vitro* and *in vivo* antiviral effects of salinomycin

Yejin Jang,[a] Jin Soo Shin,[a,b] Yi-Seul Yoon,[a] Yun Young Go,[a,c] Hye Won Lee,[a*] Oh Seung Kwon,[a,c] Sehee Park,[d] Man-Seong Park,[d] Meehyein Kim[a,c]

[a]Virus Research Group, Korea Research Institute of Chemical Technology (KRICT), Daejeon, Republic of Korea

[b]Department of Biological Sciences, Korea Advanced Institute of Science and Technology (KAIST), Daejeon, Republic of Korea

[c]Department of Medicinal Chemistry and Pharmacology, Korea University of Science and Technology (UST), Daejeon, Republic of Korea

[d]Department of Microbiology, Institute for Viral Diseases, College of Medicine, Korea University, Seoul, Republic of Korea

[*] Present address: Center for Infectious Disease Research, Korea Centers for Disease Control and Prevention (KCDC), Cheongju, Republic of Korea

Corresponding author

Meehyein Kim, Ph.D.

Virus Research Group, Therapeutics and Biotechnology Division, Korea Research Institute of Chemical Technology, 141 Gajeongro, Yuseong, Daejeon 34114, Republic of Korea

E-mail: mkim@krict.re.kr; Telephone: 82-42-860-7540; Fax: 82-42-860-7400

ABSTRACT

Screening of chemical libraries with 2,000 synthetic compounds identified salinomycin as a hit against influenza A and B viruses with 50% effective concentrations ranging from 0.4 to 4.3 μM in cells. This compound is a carboxylic polyether ionophore that exchanges monovalent ions for protons across lipid bilayer membranes. Monitoring the time course of viral infection showed that salinomycin blocked nuclear migration of viral nuclear protein (NP) that is the most abundant component of the viral ribonucleoprotein (vRNP) complex. It caused cytoplasmic accumulation of NP, particularly within perinuclear endosomes, during virus entry. This was primarily associated with failure to acidify the endosomal-lysosomal compartments. Similar to amantadine (AMT), proton channel activity of viral matrix protein 2 (M2) was blocked by salinomycin. Using purified retroviral Gag-based virus-like particles (VLPs) with M2, it was proved that salinomycin directly affect the kinetics of a proton influx into the particles but in a different manner from that of AMT. Notably, oral administration of salinomycin together with the neuraminidase inhibitor oseltamivir phosphate (OSV-P) led to enhanced antiviral effect over either compound used alone in influenza A virus-infected mouse models. These results provide a new paradigm for developing antivirals and their combination therapy that control both host and viral factors.

46 **IMPORTANCE**

47 Influenza virus is a main cause of viral respiratory infection in humans as well as
48 animals, occasionally with high mortality. Circulation of influenza viruses resistant to the matrix
49 protein 2 (M2) inhibitor, amantadine, is highly prevalent. Moreover, detection frequency of
50 viruses resistant to the neuraminidase inhibitors including oseltamivir-phosphate (OSV-P) or
51 zanamivir is also increasing. These issues highlight the need for discovery of new antiviral
52 agents with different mechanisms. Salinomycin as the monovalent cation-proton antiporter
53 exhibited consistent inhibitory effects against influenza A and B viruses. It plays multifunctional
54 roles by blocking endosomal acidification and by inactivating the proton transport function of
55 M2, the key steps for influenza viral uncoating. Notably, salinomycin resulted in marked
56 therapeutic effects in influenza virus-infected mice when combined with OSV-P, suggesting that
57 its chemical derivatives could be developed as an adjuvant antiviral therapy to treat influenza
58 infections resistant or less sensitive to existing drugs.

INTRODUCTION

Influenza viruses belonging to the family *Orthomyxoviridae* harbor a genome comprising eight-segmented negative sense RNAs. These viruses are classified into three types, A, B, and C, based on variations in the nucleoprotein (NP) and matrix protein 1 (M1) (1). Influenza A viruses are further divided into subtypes distinguished by the antigenic properties of two viral surface glycoproteins, hemagglutinin (HA) and neuraminidase (NA). Although inactivated vaccines and antiviral available to prevent or treat influenza A and B, these viruses still cause seasonal epidemics with 300,000–500,000 deaths worldwide every year (World Health Organization (http://www.who.int/mediacentre/factsheets/fs211/en/) (2). Viral infection is initiated by binding of HA to sialic acid receptors on the epithelial cell surface, followed by engulfment of viral particles within endocytic vesicles. For the successful viral infection, it is essential for the precursor HA0 to be enzymatically cleaved into two subunits, HA1 and HA2, that are linked by a single disulfide bond (3). The low pH environment of the endosome activates the proton channel function of matrix protein 2 (M2), which is necessary for release of viral ribonucleoprotein (vRNP) complexes, comprising viral RNA, NP, and viral RNA polymerases PB2, PB1, and PA, from the M1 matrix layer. It also induces irreversible conformational changes in HA, which lead to HA2-mediated fusion between the viral envelope and the endosomal membrane (4-6). Each free vRNP is transported to the nucleus, where viral RNA transcription and replication occur. Newly synthesized vRNPs are bound to M1 again, which interacts with the nuclear export protein [NEP; formally called nonstructural protein 2 (NS2)] and is exported to the cytoplasm via a chromosomal maintenance 1-dependent pathway (7). Assembly of influenza viral particles

requires successive migration of these vRNPs beneath the apical plasma membrane, where all structural protein components of HA, NA, M2, and M1 are arrayed. At the final stage of the viral life cycle, progeny virions bud from the cell surface with the help of NA, which cleaves terminal sialic acid from cell surface glycans.

Two classes of antivirals that target influenza viral proteins NA and M2 have been approved by the U.S. Food and Drug Administration (8, 9). The NA inhibitors, oseltamivir phosphate (OSV-P) and zanamivir, are used globally to treat influenza infection. Although they have potent broad-spectrum efficacy, emergence of drug-resistant viruses harboring mutations in NA is a major concern. Recently, sporadic human infections caused by oseltamivir-resistant seasonal or influenza A pandemic (H1N1) 2009 viruses were reported (10). Adamantanes (amantadine and rimantadine), which are proton channel M2 inhibitors, can be used to treat influenza A, but not B. However, because almost 100% of currently circulating influenza A viruses are resistant to these drugs, M2 inhibitors are not recommended (11). Adamantane resistance is mainly conferred by Val-27-Ala (V27A) and/or Ser-31-Asn (S31N) mutations within M2. To overcome the limitations associated with reduced antiviral efficacy, synthesis of chemical derivatives of adamantanes, which are active against the mutant M2 proteins of influenza A viruses, was investigated (12, 13). Nevertheless, their therapeutic activity was still restricted to influenza A virus. This is not surprising since influenza A virus M2 and influenza B virus M2 have little structural or sequence homology despite their functional similarity as proton channels (14, 15). Thus, antiviral compounds with a high barrier to resistance that inhibit M2 of both types are required.

Ionophores are small molecules that facilitate movement of specific ions across lipid

bilayer membranes; they are divided into electrogenic or electroneutral ionophores (16). Electrogenic ionophores, such as valinomycin, carbonyl cyanide *m*-chlorophenylhydrazone (CCCP), and carbonyl cyanide 4-(trifluoromethoxy)phenylhydrazone (FCCP), transfer a net charge across the membrane. In contrast, electroneutral ionophores, also called carboxyl polyether ionophores, such as monensin, A23187, nigericin, salinomycin, and lasalocid acid, form zwitterionic complexes with cations and facilitate electrically neutral cation exchange diffusion. Polyether ionophores are regarded as promising bioactive molecules due to their broad-spectrum anti-cancer and anti-bacterial properties (17, 18). They were additionally reported to possess antiviral activity: zinc ionophores (pyrithione and hinikitiol) are active against picornavirus, herpes simplex virus, or coronavirus (19-21), and the sodium-selective carboxylic ionophore monensin is active against mouse polyomavirus (22). Monensin was suggested to affect the processing and intracellular transport of HA at first, but it was also proposed to stimulate the proton channel of the influenza viral M2 (23, 24).

Here, we found that another monovalent ionophore, salinomycin, which was identified through high-throughput screening (HTS) of chemical libraries, suppressed influenza A and B virus infection in cell culture. Its antiviral activity was mediated via inhibition of endosomal acidification and M2 proton channel activity simultaneously. It is noteworthy that oral administration of salinomycin together with OSV-P into mice that were infected with influenza A virus resistant to AMT or double resistant to AMT and OSV-P showed improved antiviral efficacy when compared to their separate treatments. If a toxicity-attenuated monovalent ionophore is discovered through chemical modifications, this combination approach might provide an alternative for patients infected with influenza viruses that show reduced or no

sensitivity to current existing antivirals.

RESULTS

Activity of salinomycin against influenza viruses

We screened 2,000 chemicals for activity against influenza viruses, A/Puerto Rico/8/1934 (PR8; H1N1), A/Hong Kong/8/1968 (HK; H3N2), and B/Lee/1940 (Lee), by examining cytopathic effects (CPEs) in a 3-(4,5-dimethylthiazol-2-yl)-2,5-diphenyltetrazolium bromide (MTT)-based assay with Z' values >0.6 (25). Of the 9 primary hits that maintained >80% viability of influenza A or B virus-infected Madin-Darby canine kidney (MDCK) cells at a concentration of 20 μM, three compounds, including atovaquone, Evans blue, and salinomycin, were characterized to suppress viral replication in a dose-dependent manner with selectivity indices >10 (Table 1). The antiviral tests with amantadine hydrochloride (AMT), ribavirin (RBV), and oseltamivir carboxylate (OSV-C) used as positive controls ensured the reliability of the assay. As shown in our previous report, wild-type PR8 virus was resistant to AMT (26). Sequence analysis of viral cDNA followed by alignment to a reference sequence from GenBank (accession no. EF467824) revealed that PR8 M2 possesses amino acids Ala 27 (A27) and Asn 31 (N31), which confer AMT resistance. Moreover, among the three hits, salinomycin that has five ether rings and a terminal carboxylic acid (Fig. 1A) exhibited the most potent activity against the influenza strains, PR8, HK and Lee, tested for high 50% effective concentration (EC_{50}) values ranging from 0.4 to 0.8 μM and the 50% cytotoxic concentration (CC_{50}) of 35.6 μM (Table 1 and Fig. 1B). To evaluate its broad-spectrum antiviral activity, CPE assay was performed repeatedly against seventeen additional influenza viruses including seven A/H1N1 strains (Table 2), six A/H3N2, A/H3N8 or A/H9N2 strains (Table 3) and four B strains (Table 4). These results showed that salinomycin has inhibitory effects against wild-type influenza A viruses as well as

148 AMT- or OSV-resistant strains or even against avian influenza A/H3N8 or A/H9N2 viruses with
149 EC_{50} values between 0.4 to 4.3 μM. Western blot analysis again demonstrated that salinomycin
150 suppressed NP, HA, M1, and M2 expression of PR8 in a dose-dependent manner (Fig. 1C).
151 Consistent with this result, a plaque assay verified the salinomycin-mediated reduction in the
152 number of infectious influenza viral particles from the culture supernatant on days 1 and 2 post-
153 infection (p.i.) (Fig. 1D). These data indicate that salinomycin is active against both influenza A
154 and B viruses.
155
156 **Changes in nuclear localization of NP**
157 Next, we evaluated which stage of the virus life cycle is targeted by the hit compound.
158 To investigate the underlying mechanism(s) of action, we added the test compounds to cells at
159 different stages (e.g., during or after adsorption) and monitored changes in antiviral activity by a
160 plaque reduction assay. We found that incubating virus with salinomycin at 4°C for 1 h (viral
161 adsorption) had no effect on viral growth, whereas epigallocatechin gallate (EGCG) (a viral entry
162 blocker) suppressed virus infection markedly by 92.3% (Fig. 2A) (25). It is noteworthy that at
163 35°C, a temperature at which PR8 follows the typical viral life cycle, salinomycin interfered with
164 viral infectivity in reversely proportional to the time of addition. In other words, its treatment for
165 0-5 or 1-5 h p.i. resulted in considerable and efficient inhibition, with a reduction in plaque
166 numbers of 83.2% and 79.5%, respectively. However, treatment at later times (2-5 or 4–5 h p.i.)
167 suppressed PR8 replication by only 60.8% and 53.4%, respectively. Taken together, the time of
168 addition study indicated that salinomycin could target the early stage of the influenza viral life
169 cycle, but not the very first step such as adsorption or attachment of viral particles to the cell

surface receptors.

To visualize the effect of salinomycin on the early stage, we tested the intracellular distribution of NP as a representative of vRNPs by confocal microscopy at 4 h p.i. (Fig. 2B). At this time point, vRNPs are fully transported to the nucleus through receptor-mediated endocytosis to initiate RNA replication and transcription there (Fig. 2B, DMSO). Interestingly, salinomycin induced cytoplasmic retention of vRNPs, evidently indicating that it affected their nuclear migration. Meanwhile, a control image of EGCG-treated cells revealed no NP signals as a result caused by suppression of membrane binding or penetration of virions. Relatively weak intensities of nuclear NP in RBV-treated cells mean the inhibitory effect on viral RNA synthesis but not on vRNP shuttling. Hence, these data suggested that salinomycin restricts nuclear transport of vRNPs during the virus entry step.

Endosomal escape ability of influenza vRNPs

Salinomycin is a monovalent cation ionophore isolated from *Streptomyces albus* and is presumed to prevent formation of proton gradients by vacuolar ATPase (V-ATPase) existing in intracellular organelles and at the plasma membrane (27, 28). Therefore, we asked whether this electroneutral ionophore neutralizes acidic intracellular compartments such as lysosomes, endosomes, or the Golgi apparatus in cells. Live MDCK cells were stimulated with salinomycin for 1 h, by using bafilomycin A1 (a V-ATPase inhibitor) or chloroquine (a lysosomal lumen alkalizer) as positive controls. Intracellular vesicles were stained with acridine orange to monitor pH change (Fig. 3). Emission of red fluorescence highlighted low pH organelles in mock cells (Fig. 3, mock). By contrast, no or weak red fluorescence was observed in the cytoplasm of cells

192 exposed to salinomycin, being similar to the cells exposed to bafilomycin A1. Moreover,
193 yellow/green fluorescence was detected in chloroquine-treated cells. This result indicated that the
194 antiviral ionophore raised the pH of acidic cytoplasmic compartments. Thus, the data suggested
195 that salinomycin plays a role as a negative competitor of the cellular proton channels and
196 eventually prevents acidification of the endosome-lysosome system, which is prerequisite for
197 membrane fusion by HA2 and for viral uncoating by M2.

198 Next, we investigated whether salinomycin-mediated inhibition of endocytic vesicle
199 acidification affects endosomal trafficking pathways of influenza virus vRNPs. To explore this,
200 A549 cells were infected at a high multiplicity of infection (MOI, 10) of PR8 in the absence or
201 presence of salinomycin, in which protein synthesis was arrested by addition of cycloheximide
202 (CHX). Cells were incubated for 8 h at 35°C to allow sufficient nuclear import of incoming
203 vRNPs and then co-stained for viral NP and early endosome antigen 1 (EEA1, an early
204 endosome marker; Fig. 4A) or lysosomal-associated membrane protein 1 (LAMP1, a late
205 endosome marker; Fig. 4B). Confocal microscopy visualized that NP (or vRNP) released from
206 both the early and late endosomes migrated to the nucleus (Fig. 4A and B, left columns).
207 However, salinomycin induced aberrant distribution of NP with accumulation in the cytoplasm
208 (Fig. 4A and B, right columns). Addition of CHX supported that the NP localized in the
209 cytoplasm was derived from input influenza virions, rather than from newly synthesized, nuclear
210 exported viral products. Interestingly, NP complexed with early or late endosomes gathered
211 around the perinuclear region (Fig. 4, merged images). We concluded that salinomycin-mediated
212 defects in endosomal acidification may be linked with the failure of vRNPs to escape from early
213 or late endosomal vesicles, thereby having an adverse effect on endosomal recycling.

Effects on the viral proton channel M2

Next, we asked whether salinomycin influences the function of the viral proteins such as M2 or HA2, that are involved in endosomal escape of vRNPs. To quantify the proton channel activity of M2, we prepared retroviral Gag-based VLPs combined with PR8 M2 by ultracentrifugation of culture supernatants from transfected 293T cells. In this case, AMT-sensitive mutant PR8 M2 (PR8M2-S), which harbors amino acid substitutions V27 and S31, and AMT-resistant wild-type PR8 M2 (PR8M2-R), which harbors amino acids A27 and N31, were independently incorporated into null VLPs to compare their susceptibility to salinomycin. Dynamic light scattering (DLS) analysis confirmed that their mean diameters were 268.3 ± 8.3 nm for null, 256.8 ± 2.5 nm for PR8M2-S and 238.3 ± 5.9 nm for PR8M2-M VLPs with homogeneity in size and shape (data not shown). Western blot analysis showed that the murine leukemia virus (MLV) Gag-derived capsid protein p30 (CA) was included in all VLP preparations; however, M2 was incorporated into PR8M2-S and PR8M2-R chimeric VLPs selectively (Fig. 5A). Individual VLP samples were exposed to acidic conditions (pH 4.5) and real-time activity of pH-gated proton channels was monitored using a fluorescent dye sensitive to membrane potential (Fig. 5B). At the low pH, null VLPs exhibited a basal increase in fluorescence, indicating slow migration of protons across the membrane (Fig. 5B, upper left panel). This is likely caused by cellular proton pumps incorporated within the VLP membrane or by non-selective proton diffusion. The basal proton channel activity of null VLPs did not respond to either AMT or salinomycin. However, the electrogenic ionophore FCCP complexed with VLPs led to a sudden increase in proton transport at 36 s after exposure to low pH buffer. This

proton channel activity of FCCP VLPs fell gradually, eventually reaching equilibrium (Fig. 5B, upper right panel). It indicated that FCCP could transport protons bidirectionally. It is noteworthy that salinomycin compensated the effect of FCCP, suggesting that the activity of an electroneutral ionophore is more dominant than that of an electrogenic ionophore when they coexist. In addition, there was no difference between DMSO-treated and AMT-treated FCCP VLPs with respect to proton migration kinetics. Meanwhile, consistent with a previous report (29), VLPs spiked with PR8M2-S and PR8M2-R proteins allowed proton influx under acidic conditions (Fig. 5B, lower left and right panels, respectively). As expected, PR8M2-S VLPs were sensitive to AMT, whereas PR8M2-R VLPs were not, confirming the feasibility of the M2 activity assay (compare red lines in the lower panels of Fig. 5B). We found that salinomycin suppressed M2 proton channel activity efficiently, independent of its sensitivity to AMT (compare blue lines in the lower panels of Fig. 5B). We calculated that it suppressed PR8M2-S and PR8M2-R function by 54% and 72%, respectively, at the end point (5 min) of the experiment (Fig. 5C). Similarly, the function of M2 derived from influenza B virus Lee strain (LeeM2) was inhibited by salinomycin but not AMT (Fig. 5A and D). These results suggested that salinomycin expressed antiviral activity against influenza A and B viruses in cells by hindering endocytic pathways in two ways: by preventing acidification of endosomal vesicles (Fig. 3) and by blocking M2-mediated proton migration from virus-carrying endosomes into virions (Fig. 5).

Another putative target, HA2, was investigated whether its membrane fusion activity is regulated by salinomycin. PR8-infected Vero E6 cells were incubated with the antiviral hit by using an HA2-specific antibody as a control to compare changes in HA-mediated cell-cell fusion efficiency in acidic buffer (Fig. 6). Microscopic images revealed large syncytia with multiple

nuclei upon influenza virus infection, at pH 5.6. In contrast to anti-HA2 antibody which is a fusion blocker, efficiency of the large syncytia formation with multiple nuclei was not affected by salinomycin (Fig. 6A). From sixteen randomly selected images, it was determined that the total number of nuclei in syncytia per field was reduced by 61.4% and 79.3% by 0.5 μg/ml and 5.0 μg/ml of the anti-HA2 antibody with statistical significance, but not by salinomycin (Fig. 6B). Thus, HA2 that functions as a fusion protein during endosomal uncoating did not seem to be a primary target of the electroneutral ionophore, salinomycin.

Antiviral activity *in vivo*

Prior to *in vivo* antiviral study, we investigated whether the combination treatment of salinomycin with an NA inhibitor, OSV, could have advantage of synergistic interaction. The antiviral effects of salinomycin, OSV-C, and a combination of both compounds were compared under a multistep condition by CPE assay. In this condition, EC_{50} values of salinomycin and OSV-C against wild-type PR8 were 1.81 and 0.07 μM, while those against recombinant PR8 with H275Y mutation in NA [named rgPR8(H275Y)] rescued by reverse genetics were 2.37 and 3.52 μM (data not shown). Isobologram analysis revealed that their combination was synergistic as the means of the sums of fractional inhibitory concentrations at EC_{50} levels (FIC_{50}) were 0.79 against wild-type PR8 (Fig. 7A and B) and 0.63 against rgPR8(H275Y) (Fig. 7C and D).

Finally, we examined the anti-influenza virus activity of salinomycin or its combination with OSV-P in a mouse model. BALB/c mice were inoculated intranasally with five 50% mouse lethal doses (MLD_{50}) of the mouse-adapted PR8 (maPR8) (Fig. 8A). Our preliminary study revealed that upon oral administration with salinomycin at doses of 1, 5, 10, 20, and 50 mg/kg

per day for 6 days had no therapeutic effect: the body weight of infected mice failed to return to normal and in addition, it did not increase mean survival time when compared with those in the virus-only group (Fig. 8B, C, and data not shown). In a positive control group, daily treatment with OSV-P (10 mg/kg) mitigated virus-induced loss of body weight, resulting in body weight recovery on day 8 and 100% survival at the end point. By contrast, a lower dose (0.1 mg/kg) did not show satisfactory therapeutic activity, showing 0% survival. Strikingly, combination of salinomycin (10 mg/kg) and OSV-P (0.1 mg/kg) led to significant attenuation of infection-associated body weight loss (Fig. 8B). Moreover, this combination improved survival rates up to 80% (Fig. 8C). To further investigate whether this enhanced antiviral effect *in vivo* is reproducible in another mouse model, mice were infected with an OSV-P-resistant influenza virus, rgK/09Δ(H275Y), where the H275Y mutation was reverse genetically introduced into the stalk-truncated NA of the mouse-adapted rgA/Korea/09/2009Δ53-60 strain (30). As expected, salinomycin (10 mg/kg) alone did not show antiviral activity in this model (data not shown). Compared to maPR8, a 10-fold higher dose of OSV-P (100 mg/kg) was consumed to apparently reduce body weight loss or to completely survive rgK/09Δ(H275Y)-infected mice (Fig. 9). There was no statistical significance in body weight changes between the OSV-P (10 mg/kg)-only group and its combination with salinomycin (Fig. 9A). However, this combination improved mean survival rates from 60% to 100% (Fig. 9B). Notably, therapeutic effect was most potent in the combination of salinomycin with the higher dose of OSV-P (100 mg/kg). Body weight recovery induced by OSV-P (100 mg/kg) was accelerated in the presence of salinomycin with statistical significance between days 4 and 12 p.i., resulting in complete survival in both groups (Fig. 9). It should be also stressed that both strains used for *in vivo* antiviral studies are resistant

to AMT (Tables 1 and 2). Taken together, these studies indicated that salinomycin alone did not induce a marked therapeutic effect, but it was able to boost the antiviral activity of OSV-P when the latter was used at an otherwise ineffective dose or even against an AMT- and OSV-P-resistant strain. This enhanced antiviral effect might be attributed to targeting of various steps of the virus life cycle by two different inhibitors, one that blocks endosomal acidification and M2-mediated vRNP dissociation from the M1 shell, and the other that suppresses NA-dependent progeny virion release.

DISCUSSION

Several reports suggested that ionophores affect replication of influenza virus. For example, an electrogenic ionophore, CCCP, acts as an artificial M2-like channel to deliver protons to viral particles in influenza virus-infected cells, thereby increasing viral infectivity (31). Similarly, we and others showed that FCCP, a chemical analogue of CCCP, stimulates proton influx into retroviral Gag-based VLPs (29). Among the electroneutral ionophores, monensin is the most actively studied compound to evaluate its role as a monovalent cation/proton antiporter during influenza viral infection. However, those results were contradictory with respect to viral replication and infectivity. For example, Bron *et al*. used purified influenza virus and fluorescent pyrene-labeled liposomes to demonstrate that monensin promoted membrane fusion activity. This was an advantage for viral infection; actually a fusion assay showed that monensin was in a reverse manner to that of the M2 blocker, AMT (24). By contrast, Edwardson showed that monensin acts as an inhibitor of terminal glycosylation of HA, eventually interfering with its transport to the plasma membrane via the stacked Golgi cisternae during viral assembly (23). Similarly, Amorim *et al.* reported that monensin-mediated disruption of vesicular trafficking altered vRNA transport, leading to detection of perinuclear vRNA foci and nuclear retention of NP (32). Here, we observed that salinomycin inhibited influenza A and B viruses, but via a unique mode of action different from those proposed previously. To the best of our knowledge, this is a first paper to suggest that salinomycin, a representative natural polyether ionophore, targets the uncoating step of an enveloped virus. The findings highlight its multifunctionality: the compound not only neutralizes endosomal and lysosomal vesicles but also nullifies the proton channel activity of viral M2. We studied whether the electroneutral ionophore additionally could

inhibit HA2 fusion activity, another key molecule involved in viral uncoating. However, HA2 was not a direct target because HA-mediated cell-cell fusion under acidic conditions was not influenced by salinomycin (Fig. 6). Nevertheless, it is difficult exclude the possibility that it affects the fusion step indirectly by blocking endosomal acidification and by precluding conformational changes in HA.

A report demonstrated the potential benefits of combination therapy of favipiravir (T-705; a viral RNA-dependent RNA polymerase inhibitor) and OSV-P; either compound was ineffective at suboptimal doses, while their combination led to a significant increase in body weight and survival of mice infected with influenza A virus (33). Similarly, triple combination of OSV, AMT and RBV displayed synergistic antiviral activity against multiple influenza viruses (34-36). In agreement with these, we found that oral administration of salinomycin (10 mg/kg per day) and OSV-P (0.1 mg/kg per day) generated therapeutic effects in influenza virus-infected mice; neither drug showed therapeutic efficacy at the same doses when used alone (Fig. 8). The improved antiviral effect might be attributed to inhibition of multiple steps essential for virus replication, such as endosomal acidification, M2 proton channel function, and NA-mediated release of virus from the host cell. Currently, the monovalent ionophore salinomycin is approved for veterinary use as an antiprotozoal agent and is used to treat coccidiosis in poultry in addition to monensin, narasin and lasalocid (37, 38). Although they were proposed to be effective against human cancers and infectious diseases, their potential toxicity and/or side effects limited their clinical use (39-41). We found that its combination with OSV-P did not cause changes in body weight, behavior, or food uptake of normal mice (data not shown). However, a more systematic toxicology study may be required to examine the presence of delayed or latent toxicity to

mammals. We also expect that toxicities could be alleviated by synthesizing less cytotoxic chemical derivatives as tried in previous reports (42, 43) or by conjugating the active compound to a delivery vehicle specific for virus-infected lung epithelial cells. Particularly, Brogström *et al*. suggested that modifications to the C20 hydroxy group within the C-ring of salinomycin (Fig. 1A) would be beneficial in the context of selectivity (43). The combined therapeutic approach with salinomycin derivatives and a lower-dose NA inhibitor may also be valuable when the stockpiles of OSV-P are insufficient to respond to an influenza pandemic or when OSV-resistant viruses are circulating globally. Or it might be useful to protect transmission of avian influenza virus from poultry to humans or among poultry by treating chickens or ducks with salinomycin in combination with different antivirals, as it could mitigate the risk of antiviral resistance emergence due to a heightened genetic barrier of multiple mutations (44, 45).

Moreover, the influenza viral strains maPR8 and rgK/09Δ(H275Y) used for the *in vivo* antiviral studies herein with the natural occurring carboxylic polyether ionophore are AMT-resistant (Table 2). Associated with this, cell culture-based antiviral assays revealed that salinomycin had broad-spectrum antiviral effects against all influenza A and B viral strains independent of their AMT-sensitivity (Tables 1 to 4). Functional analysis using purified VLPs spiked with M2 further defined that it inhibited viral M2, irrespective of its responsiveness to AMT (Fig. 5). The results suggest that salinomycin controls fundamentally the proton channel activity of M2 via a mechanism different from that of AMT, an M2 blocker recognizing the ion channel pore and the lipid face of the pore within M2 (46). It is possible that similar to AMT, the ionophore binds directly to a third site within M2. However, based on the biological roles of electroneutral ionophores, it might be more reasonable to explain that it facilitates counter-

transport of protons and Na^+ ions, which exist abundantly (at a concentration of about 150 mM) under physiological conditions, bidirectionally across lipid bilayers to reach an ionic equilibrium. In the future, we are going to explore antiviral effects of salinomycin against other enveloped viruses that enter cells via endosome-mediated endocytosis and to investigate anti-influenza viral activity of detoxified salinomycin derivatives. The findings here provide a comprehensive methodology for investigating antiviral effects of ionophores by using salinomycin as a probe and a new paradigm for combination therapy simultaneously targeting viral proteins and a cellular machinery critical for virus uncoating.

383 **MATERIALS AND METHODS**

384

385 **Cells and viruses**

386 MDCK cells, human lung adenocarcinoma A549, human embryonic kidney 293T cells,
387 and African green monkey kidney epithelial Vero E6 cells were purchased from the American
388 Type Culture Collection (ATCC, Manassas, VA). MDCK and A549 cells were maintained in
389 minimum essential medium (MEM; Hyclone, Logan, UT) and in RPMI-1640 medium (Hyclone),
390 respectively, supplemented with 10% fetal bovine serum (FBS; Hyclone) at 37°C. 293T and Vero
391 E6 cells were cultured in Dulbecco's Modified Eagle's Medium (DMEM; Hyclone)
392 supplemented with 10% FBS.

393 Influenza viruses, including PR8 (A/H1N1), HK (A/H3N2), and Lee (B), were
394 purchased from ATCC. Recombinant rgPR8(H275Y) virus was generated by reverse genetics and
395 site-directed mutagenesis of H275Y in NA of PR8 (25, 47). At the Dr. M. Park's laboratory
396 (Korea University, Seoul, Republic of Korea), another recombinant virus, rgK/09Δ(H275Y), was
397 created by genetically substituting His at amino acid 275 with Tyr in NA of the
398 rgA/Korea/09/2009Δ53-60 strain, in which an NA stalk was truncated during mouse adaptation
399 (30). Another mouse-adapted influenza virus maPR8 was a kind gift from H. J. Kim (Chung-Ang
400 University, Seoul, Republic of Korea) (26). PR8, HK, rgPR8(H275Y) and maPR8 were
401 amplified by infection of 10-day-old embryonated SPF chicken eggs at 37°C for 3 days. Lee was
402 infected into MDCK cells for amplification at 35°C for 3 days in serum-free MEM in the
403 presence of 2 μg/ml TPCK-treated trypsin (Sigma-Aldrich, St. Louis, MO). Other influenza
404 viruses used for antiviral assay were obtained from ATCC, Korea Centers for Disease Control

405 and Prevention (KCDC), and Korea Veterianry Culture Collection (KVCC), and amplified
406 according to the suppliers' instructions (26). Viruses were harvested by centrifugation of
407 allantoic fluid or culture medium at 1,300 × *g* for 10 min. They were stocked at -70°C, and viral
408 titers were determined in a plaque assay (48).
409
410 **Plasmids**
411 PR8 M2 cDNA (GenBank accession no. EF467824), which encodes two amantadine-
412 resistant amino acid sequences, A27 and N31, was synthesized (Bioneer Corp. Daejeon,
413 Republic of Korea) and cloned into the *Nhe*I and *Bam*HI sites of pcDNA 3.1/*myc*-His(-) A
414 (Invitrogen, Carlsbad, CA); the resulting construct was named pcDNA-PR8M2-R. The plasmid
415 pcDNA-PR8M2-S, which expresses amantadine-sensitive PR8M2 harboring amino acids V27
416 and S31 was prepared using the same method. The plasmid pcDNA-LeeM2 was also cloned by
417 gene synthesis of M2 cDNA derived from the Lee strain (GenBank accession no. DQ792900).
418 The retroviral packaging plasmid pCgp, which expresses MLV Gag-Pol, was a kind gift
419 from Paula M. Cannon (University of Southern California, CA) (49).
420
421 **Chemicals used for antiviral assays**
422 A chemical library comprising 2,000 small molecules, all collected from the
423 Microsource Spectrum Collection (MicroSource Discovery Systems, Gaylordsville, CT), the
424 Prestwick Chemical Library (Prestwick Chemical, Inc., Washington, DC), and Tocriscreen
425 bioactive compounds (Tocris Bioscience, Bristol, UK), was provided by the Korea Chemical
426 Bank (Daejeon, Republic of Korea).

AMT and RBV, which are viral M2 and RNA polymerase inhibitors, respectively, were purchased from Sigma-Aldrich. The NA inhibitor OSV-C and its prodrug OSV-P were obtained from US Biological (Swampscott, MA) and Hanmi Pharmaceutical Co. (Gyeonggi-do, Republic of Korea), respectively. The test compound salinomycin and the control compound EGCG were purchased from Sigma-Aldrich. The purity of salinomycin and EGCG was over 95%. Except for screening of the chemical library, high purity compound was used in all experiments. Other hit compounds, Evans blue and atovaquone, were also purchased from Sigma-Aldrich for re-evaluating their antiviral activity.

Cytopathic inhibition assay

For high-content screening of the chemical library, MDCK cells were seeded in 96-well plates (3×10^4 cells per well) and infected with individual influenza viruses at an MOI of 0.001 in serum-free MEM for 1 h at 35°C or 37°C. After washing with phosphate-buffered saline (PBS), cells were treated with each of the 2,000 compounds diluted in MEM (final concentration, 20 μM) containing 2 μg/ml TPCK-trypsin. After incubation for 3 days at the same temperature for viral infection, inhibition of influenza virus-induced CPEs was measured by addition of 2.5 mg/ml MTT (50). Dose responses to the selected hit compounds or the reference antiviral compounds were measured by treating mock- or virus-infected cells with serial dilutions of test compounds. The CC_{50} and EC_{50} values were calculated using GraphPad Prism 6 software (GraphPad, La Jolla, CA).

Western blot analysis

PR8-infected MDCK cells were treated with increasing concentrations of salinomycin (0.1, 1.0, and 10.0 μM) or OSV-C (0.1 μM), and culture lysates were harvested 1 day later. Lysates were loaded onto 12% SDS-PAGE gels (30 μg total protein per well) and electro-transferred to a PVDF membrane. Viral NP, HA, M1, and M2 proteins were detected using mouse anti-NP (catalog no. 11675-MM03; Sino Biological, Beijing, China), rabbit anti-HA2 (catalog no. 86001-RM01; Sino Biological), mouse anti-M1 (catalog no. sc-57881; Santa Cruz Biotechnology, Santa Cruz, CA), and mouse anti-M2 (catalog no. sc-32238; Santa Cruz Biotechnology) antibodies, respectively. Cellular β-actin was used as a loading control and detected with a mouse anti-β-actin antibody (catalog no. A1987; Sigma-Aldrich). Horseradish peroxidase (HRP)-conjugated goat anti-mouse or anti-rabbit secondary antibodies were used to probe membrane-bound primary antibodies (Thermo Scientific, Waltham, MA). After addition of a chemiluminescent HRP substrate (SuperSignal West Pico Chemiluminescent Substrate; Pierce, Rockford, IL), images were obtained using a LAS-4000 Luminescent Image Analyzer (Fujifilm, Tokyo, Japan).

To detect M2-His fusion proteins incorporated into MLV-based VLPs, the purified, 500-fold concentrated samples (final volume, 150 μl) were loaded on a 12% SDS-PAGE gel (2 μl per well). Gag-derived p30 capsid (CA) protein was probed with an anti-Gag antibody (cat. no. R187, ATCC) and a secondary HRP-conjugated goat anti-rat IgG. M2 proteins fused with a myc-His tag was visualized by incubation with an anti-6× His tag antibody (catalog no. ab18184, Abcam) and an HRP-conjugated goat anti-mouse antibody.

Plaque reduction assay

MDCK cells in 6-well plates were inoculated with PR8 (MOI, 0.001) under serum-free culture conditions in the presence of DMSO (0.2%, v/v) or increasing concentrations of salinomycin (0.1, 1.0, and 10.0 μM) and 0.1 μM OSV-C. Cells were cultured at 35°C and supernatants were harvested on days 1 and 2 p.i. To titrate infectious viral particles, fresh MDCK cells were seeded into 48-well plates. On the next day, 10-fold serial dilutions (10^{-1} to 10^{-6}) of the virus inoculum were treated into MDCK cells for 1 h. After washing with PBS, the cell monolayers were overlaid with overlay medium [MEM containing 0.5% carboxymethylcellulose (CMC; Sigma-Aldrich) and 2 μg/ml TPCK-trypsin] and incubated for 3 days at 33°C. Viral plaques were visualized by staining with crystal violet (25).

For the time of addition experiment, MDCK cells grown to confluence in 48-well plates were infected at 4°C for 1 h with PR8 in the presence of 10 μM salinomycin or EGCG (an entry blocker). After washing with PBS to remove unadsorbed virus and chemicals, the cells were treated at 35°C with media alone or with the individual compounds for additional 4 h. In parallel, virus-infected cells in the absence of the compounds were treated with the compounds sequentially at 1, 2 and 4 h p.i. At 5 h p.i., all samples were washed with PBS and incubated in overlay medium supplemented with 2 μg/ml TPCK-trypsin for plaque titration as described above.

Confocal microscopy

MDCK cells in 4-well chamber slides were infected for 4 h at 37°C with PR8 (MOI, 2.5) in the presence of DMSO (0.2%, v/v), salinomycin (10 μM), EGCG (100 μM), or RBV (100 μM,

a polymerase inhibitor). The cells were then fixed with 4% paraformaldehyde and permeabilized with 0.1% Triton X-100. After blocking with 1% BSA and 10% normal goat serum prepared in PBS, the slides were incubated overnight at 4°C with an influenza A NP-specific monoclonal antibody (catalog no. sc-80481; Santa Cruz Biotechnology). The anti-NP antibody-bound cells were subsequently labeled for 1 h at room temperature with Alexa Fluor 488-conjugated goat anti-mouse IgG (Invitrogen) and counterstained with Vectashield mounting medium containing DAPI (Vector Laboratories, Burlingame, CA). Laser scanning confocal microscopy was performed with a Zeiss LSM 700 confocal microscope. Images were analyzed using the ZEN program (Carl Zeiss, Thornwood, NY).

To measure pH changes in cytoplasmic membrane-enclosed vesicles, cells were stained with acridine orange as described previously (51). MDCK cells (8×10^4 cells per well) were cultured at 37°C in 35 mm glass-bottom dishes (Greiner Bio-One, Frickenhausen, Germany). On the next day, they were treated for 1 h at the same temperature with 100 μM salinomycin, 100 nM bafilomycin A1 (a V-ATPase inhibitor; Sigma-Aldrich), or 100 μM chloroquine (an intralysosomal pH neutralizing agent; Sigma-Aldrich). Acridine orange was added (final concentration, 4 μg/ml) and cells were examined under a confocal microscope. The excitation wavelength was 488 nm, and images were collected in two emission windows: 493–560 nm and 590–720 nm.

To investigate intracytoplasmic trapping of influenza virus NP, A549 cells seeded in 4-well chamber slides (8×10^4 cells per well) were infected with PR8 at an MOI of 10 at 4°C for 30 min. After washing with PBS, virus-infected cells were incubated at 37°C for 8 h with 0.2% DMSO or 10 μM salinomycin prepared in MEM supplemented with 10 μg/ml CHX (Sigma-

Aldrich), a protein synthesis inhibitor. The cells were then co-labeled with antibodies specific for NP and EEA1 (catalog no. sc-33585; Santa Cruz Biotechnology) or for NP and LAMP1 (catalog no. 9691: Cell Signaling Technology). NP was detected with Alexa Fluor 633-conjugated goat anti-mouse IgG (Invitrogen), whereas EEA1 and LAMP1 were detected with Alexa Fluor 488-conjugated goat anti-rabbit IgG (Invitrogen).

Purification of virus-like particles (VLPs)

VLPs containing MLV Gag together with either PR8M2-S, PR8M2-R, or LeeM2 were prepared as described previously (29) with some modifications. Briefly, VLPs were generated by co-transfection of 293T cells (3×10^7 cells seeded in 150-mm cell culture dishes) with plasmids pCgp (15 μg) plus pcDNA-PR8M2-S, -PR8M2-R or -LeeM2 (45 μg) using calcium phosphate. As a control, null VLPs were produced by transfection of cells with pCgp alone. At day 2 post-transfection, cell culture supernatants (total, 80 ml) were centrifuged through a 20% sucrose cushion at 16,500 × g for 2 h at 4°C in an SW-32Ti rotor (Beckmann Instruments, Palo Alto, CA). Pellets were resuspended in 1 ml of PBS followed by ultracentrifugation at 82,000 × g for 1 h at 4°C in an SW-60Ti rotor (Beckmann Instruments). After resuspending the pellet in 150 μl of 10 mM HEPES buffer, pH 7.5, particle homogeneity was measured using DLS (Zetasizer Nano series; Malvern Instruments, Malvern, UK). Two microliters of purified VLPs (about 500-fold concentrated) were separated and analyzed by microchip gel electrophoresis using the Agilent 2200 TapeStation system with the P200 Screen Tape (Agilent Technologies, Santa Clara, CA).

M2 proton channel assay

Proton channel activity of VLPs was measured as described previously (29). MLV Gag-derived VLPs (null) or Gag VLP-containing PR8M2-S, PR8M2-R or LeeM2 were suspended in 10 mM HEPES (pH 7.0) and 150 mM NaCl buffer supplemented with 1% FMP-Blue dye (Molecular Devices, Sunnyvale, CA). As a positive control, null VLPs were mixed with 5 μM FCCP (Sigma-Aldrich), an ionophore that transports protons across the membrane, to generate FCCP VLPs. To measure proton channel activity, each preparation (protein content, 1 μg) was placed in a 96-well black plate and preincubated for 1 h at room temperature with 100 μM AMT or salinomycin. Twenty microliters of 150 mM 2-(N-morpholino)ethanesulfonic acid (MES; Sigma-Aldrich), pH 4.5, was then added, thereby exposing each VLP to acidic conditions. Fluorescence was measured every 6 s for 5 min in a SpectraMax M3 Microplate Reader (Molecular Devices, Sunnyvale, CA) at an excitation wavelength of 530 nm and an emission wavelength of 565 nm.

Fusion assay

Formation of syncytia after viral infection was evaluated as described previously (52, 53). Vero E6 cells in a 12-well plate (3×10^5 cells/ml) were infected with PR8 at an MOI of 0.5 at 37°C without TPCK-trypsin. On the next day, virus-infected cells were stimulated with TPCK-trypsin (5 μg/ml) in DMEM at 37°C for 15 min and then incubated with 2 μM salinomycin or an anti-HA2 antibody (0.5 or 5.0 μg/ml; Sino Biological) in DMEM for additional 15 min. After washing with PBS containing 1 mM $MgCl_2$ and 0.1 mM $CaCl_2$ (PBS-CM), the cells were treated again with each compound dissolved in acidic or neutral PBS-CM (pH 5.6 or 7.0, respectively) for 15 min, in which pH was adjusted with citric acid. Cell-cell fusion was allowed to occur for 3

558 h at the same temperature in fresh DMEM containing 10% FBS. Cells were then fixed with 96%
559 ethanol, stained with Giemsa (Sigma-Aldrich), and visualized under a microscope at ×200
560 magnification.
561
562 **Determination of the two antiviral compound interaction and FIC index**
563 *In vitro* interaction of the two compounds, salinomycin and OSV-C, was assessed
564 according to a previous report (54). Prior to the combination treatment, EC_{50} value of each
565 compound was determined against different strains. Based on their EC_{50} values, salinomycin and
566 OSV-C were taken alone (5:0 and 0:5) and in a fixed ratio of 4:1, 3:2, 2:3 and 1:4. For the
567 combination assay, the top concentrations of the six solutions were prepared to allow the EC_{50} of
568 the individual compound to position around the middle point in two-fold serial dilutions and then
569 six dose-response curves were created.
570 The FIC_{50}s for each fixed dose ratio were calculated from the individual EC_{50} values
571 obtained from the dose-response curves (55). The sum of the FIC_{50}s (ΣFIC_{50}s) was represented
572 as isobolograms calculated using the equation:

$$\Sigma FIC_{50} = \left(\frac{EC_{50} \text{ of salinomycin in combination}}{EC_{50} \text{ of salinomycin alone}}\right) + \left(\frac{EC_{50} \text{ of OSV-C in combination}}{EC_{50} \text{ of OSV-C alone}}\right)$$

573 Interactions were classified as synergistic with ΣFIC_{50}s of <0.8.
574
575 ***In vivo* study of antiviral efficacy**
576 Six- to seven-week-old female BALB/c mice (five per group; Orient Bio Inc., Seongnam,
577 Republic of Korea) were infected intranasally with five MLD_{50} doses of maPR8 [corresponding

to 9.0×10^1 plaque forming units (pfu) per head] or rgK/09Δ(H275Y) (corresponding to 1.5×10^5 pfu per head). The antiviral compounds, OSV-P and salinomycin, separately and a combination of both were prepared in 0.5% CMC (Sigma-Aldrich) for oral administration. They were treated once at 4 h before and once 4 h after virus infection, followed by twice daily treatment for further 5 successive days. Changes in body weight were monitored for 15 days from virus infection. Mice that lost more than 30% of their body weight were euthanized in accordance with ethics guidelines approved by the Institutional Animal Care and Use Committee at the Korea Research Institute of Chemical Technology. Kaplan-Meier survival curves were created using GraphPad Prism 6 (GraphPad Software, San Diego, CA).

Statistical analysis

All the data are presented as the mean ± the standard deviation (SD). Comparisons between means of different groups were analyzed using an unpaired, two-tailed student's *t*-test. The *p* values below 0.05 were considered statistically significant.

592 **ACKNOWLEDGEMENTS**

593 This work was supported by the grant from KRICT (KK1803-E00), the
594 Transgovernmental Enterprise for Pandemic Influenza in Korea (TEPIK) (A103001) and UST
595 ICORE Research Program (2017IC0203). We thank the Korea Chemical Bank for providing
596 chemicals for HTS and for reporting LC-MS and NMR data.

REFERENCES

1. Palese P, Shaw ML. 2007. *Orthomyxoviridae*: the viruses and their replication, p 1647-1690. *In* Knipe DM, Howley PM (ed), Fields virology, 5th ed. Lippincott Williams and Wilkins, Philadelphia.
2. Clem A, Galwankar S. 2009. Seasonal influenza: waiting for the next pandemic. J Glob Infect Dis 1:51-6.
3. Chen J, Lee KH, Steinhauer DA, Stevens DJ, Skehel JJ, Wiley DC. 1998. Structure of the hemagglutinin precursor cleavage site, a determinant of influenza pathogenicity and the origin of the labile conformation. Cell 95:409-17.
4. Rogers GN, Paulson JC, Daniels RS, Skehel JJ, Wilson IA, Wiley DC. 1983. Single amino acid substitutions in influenza haemagglutinin change receptor binding specificity. Nature 304:76-8.
5. Skehel JJ, Wiley DC. 2000. Receptor binding and membrane fusion in virus entry: the influenza hemagglutinin. Annu Rev Biochem 69:531-69.
6. Wharton SA, Calder LJ, Ruigrok RW, Skehel JJ, Steinhauer DA, Wiley DC. 1995. Electron microscopy of antibody complexes of influenza virus haemagglutinin in the fusion pH conformation. EMBO J 14:240-6.
7. Neumann G, Hughes MT, Kawaoka Y. 2000. Influenza A virus NS2 protein mediates vRNP nuclear export through NES-independent interaction with hCRM1. EMBO J 19:6751-8.
8. De Clercq E. 2006. Antiviral agents active against influenza A viruses. Nat Rev Drug Discov 5:1015-25.

9. Hsu J, Santesso N, Mustafa R, Brozek J, Chen YL, Hopkins JP, Cheung A, Hovhannisyan G, Ivanova L, Flottorp SA, Saeterdal I, Wong AD, Tian J, Uyeki TM, Akl EA, Alonso-Coello P, Smaill F, Schunemann HJ. 2012. Antivirals for treatment of influenza: a systematic review and meta-analysis of observational studies. Ann Intern Med 156:512-24.

10. Chen H, Cheung CL, Tai H, Zhao P, Chan JF, Cheng VC, Chan KH, Yuen KY. 2009. Oseltamivir-resistant influenza A pandemic (H1N1) 2009 virus, Hong Kong, China. Emerg Infect Dis 15:1970-2.

11. Zhang Y, Liu Q, Wang D, Chen S, Wang S. 2013. Simultaneous detection of oseltamivir- and amantadine-resistant influenza by oligonucleotide microarray visualization. PLoS One 8:e57154.

12. Li F, Ma C, Hu Y, Wang Y, Wang J. 2016. Discovery of Potent Antivirals against Amantadine-Resistant Influenza A Viruses by Targeting the M2-S31N Proton Channel. ACS Infect Dis 2:726-733.

13. Rey-Carrizo M, Torres E, Ma C, Barniol-Xicota M, Wang J, Wu Y, Naesens L, DeGrado WF, Lamb RA, Pinto LH, Vazquez S. 2013. 3-Azatetracyclo[5.2.1.1(5,8).0(1,5)]undecane derivatives: from wild-type inhibitors of the M2 ion channel of influenza A virus to derivatives with potent activity against the V27A mutant. J Med Chem 56:9265-74.

14. Williams JK, Shcherbakov AA, Wang J, Hong M. 2017. Protonation equilibria and pore-opening structure of the dual-histidine influenza B virus M2 transmembrane proton channel from solid-state NMR. J Biol Chem doi:10.1074/jbc.M117.813998.

15. Williams JK, Tietze D, Lee M, Wang J, Hong M. 2016. Solid-State NMR Investigation of

the Conformation, Proton Conduction, and Hydration of the Influenza B Virus M2 Transmembrane Proton Channel. J Am Chem Soc 138:8143-55.

16. Dobler M. 1981. Ionophores and their structures. John Wiley and Sons Ltd., New York.

17. Kevin Ii DA, Meujo DA, Hamann MT. 2009. Polyether ionophores: broad-spectrum and promising biologically active molecules for the control of drug-resistant bacteria and parasites. Expert Opin Drug Discov 4:109-46.

18. Huczynski A. 2012. Polyether ionophores-promising bioactive molecules for cancer therapy. Bioorg Med Chem Lett 22:7002-10.

19. Krenn BM, Gaudernak E, Holzer B, Lanke K, Van Kuppeveld FJ, Seipelt J. 2009. Antiviral activity of the zinc ionophores pyrithione and hinokitiol against picornavirus infections. J Virol 83:58-64.

20. Qiu M, Chen Y, Chu Y, Song S, Yang N, Gao J, Wu Z. 2013. Zinc ionophores pyrithione inhibits herpes simplex virus replication through interfering with proteasome function and NF-kappaB activation. Antiviral Res 100:44-53.

21. te Velthuis AJ, van den Worm SH, Sims AC, Baric RS, Snijder EJ, van Hemert MJ. 2010. Zn(2+) inhibits coronavirus and arterivirus RNA polymerase activity in vitro and zinc ionophores block the replication of these viruses in cell culture. PLoS Pathog 6:e1001176.

22. Iacoangeli A, Melucci-Vigo G, Risuleo G. 2000. The ionophore monensin inhibits mouse polyomavirus DNA replication and destabilizes viral early mRNAs. Biochimie 82:35-9.

23. Edwardson JM. 1984. Effects of monensin on the processing and intracellular transport of influenza virus haemagglutinin in infected MDCK cells. J Cell Sci 65:209-21.

24. Bron R, Kendal AP, Klenk HD, Wilschut J. 1993. Role of the M2 protein in influenza

virus membrane fusion: effects of amantadine and monensin on fusion kinetics. Virology 195:808-11.

25. Kim M, Kim SY, Lee HW, Shin JS, Kim P, Jung YS, Jeong HS, Hyun JK, Lee CK. 2013. Inhibition of influenza virus internalization by (-)-epigallocatechin-3-gallate. Antiviral Res 100:460-72.

26. Shin JS, Ku KB, Jang Y, Yoon YS, Shin D, Kwon OS, Go YY, Kim SS, Bae MA, Kim M. 2017. Comparison of anti-influenza virus activity and pharmacokinetics of oseltamivir free base and oseltamivir phosphate. J Microbiol 55:979-983.

27. Lu D, Choi MY, Yu J, Castro JE, Kipps TJ, Carson DA. 2011. Salinomycin inhibits Wnt signaling and selectively induces apoptosis in chronic lymphocytic leukemia cells. Proc Natl Acad Sci U S A 108:13253-7.

28. Mitani M, Yamanishi T, Miyazaki Y. 1975. Salinomycin: a new monovalent cation ionophore. Biochem Biophys Res Commun 66:1231-6.

29. Sulli C, Banik SS, Schilling J, Moser A, Xiang X, Payne R, Wanless A, Willis SH, Paes C, Rucker JB, Doranz BJ. 2013. Detection of proton movement directly across viral membranes to identify novel influenza virus M2 inhibitors. J Virol 87:10679-86.

30. Park S, Il Kim J, Lee I, Bae JY, Yoo K, Nam M, Kim J, Sook Park M, Song KJ, Song JW, Kee SH, Park MS. 2017. Adaptive mutations of neuraminidase stalk truncation and deglycosylation confer enhanced pathogenicity of influenza A viruses. Sci Rep 7:10928.

31. Stauffer S, Feng Y, Nebioglu F, Heilig R, Picotti P, Helenius A. 2014. Stepwise priming by acidic pH and a high K+ concentration is required for efficient uncoating of influenza A virus cores after penetration. J Virol 88:13029-46.

685 32. Amorim MJ, Bruce EA, Read EK, Foeglein A, Mahen R, Stuart AD, Digard P. 2011. A
686 Rab11- and microtubule-dependent mechanism for cytoplasmic transport of influenza A
687 virus viral RNA. J Virol 85:4143-56.
688 33. Smee DF, Hurst BL, Wong MH, Bailey KW, Tarbet EB, Morrey JD, Furuta Y. 2010.
689 Effects of the combination of favipiravir (T-705) and oseltamivir on influenza A virus
690 infections in mice. Antimicrob Agents Chemother 54:126-33.
691 34. Nguyen JT, Hoopes JD, Smee DF, Prichard MN, Driebe EM, Engelthaler DM, Le MH,
692 Keim PS, Spence RP, Went GT. 2009. Triple combination of oseltamivir, amantadine, and
693 ribavirin displays synergistic activity against multiple influenza virus strains in vitro.
694 Antimicrob Agents Chemother 53:4115-26.
695 35. Nguyen JT, Hoopes JD, Le MH, Smee DF, Patick AK, Faix DJ, Blair PJ, de Jong MD,
696 Prichard MN, Went GT. 2010. Triple combination of amantadine, ribavirin, and
697 oseltamivir is highly active and synergistic against drug resistant influenza virus strains in
698 vitro. PLoS One 5:e9332.
699 36. Hoopes JD, Driebe EM, Kelley E, Engelthaler DM, Keim PS, Perelson AS, Rong L, Went
700 GT, Nguyen JT. 2011. Triple combination antiviral drug (TCAD) composed of
701 amantadine, oseltamivir, and ribavirin impedes the selection of drug-resistant influenza A
702 virus. PLoS One 6:e29778.
703 37. Folz SD, Lee BL, Nowakowski LH, Conder GA. 1988. Anticoccidial evaluation of
704 halofuginone, lasalocid, maduramicin, monensin and salinomycin. Vet Parasitol 28:1-9.
705 38. Kadykalo S, Roberts T, Thompson M, Wilson J, Lang M, Espeisse O. 2017. The value of
706 anticoccidials for sustainable global poultry production. Int J Antimicrob Agents

doi:10.1016/j.ijantimicag.2017.09.004.

39. Rochdi M, Delort AM, Guyot J, Sancelme M, Gibot S, Gourcy JG, Dauphin G, Gumila C, Vial H, Jeminet G. 1996. Ionophore properties of monensin derivatives studied on human erythrocytes by 23Na NMR and K+ and H+ potentiometry: relationship with antimicrobial and antimalarial activities. J Med Chem 39:588-95.

40. Kapoor A, He R, Venkatadri R, Forman M, Arav-Boger R. 2013. Wnt modulating agents inhibit human cytomegalovirus replication. Antimicrob Agents Chemother 57:2761-7.

41. Dewangan J, Srivastava S, Rath SK. 2017. Salinomycin: A new paradigm in cancer therapy. Tumour Biol 39:1010428317695035.

42. Steverding D, Antoszczak M, Huczynski A. 2016. In vitro activity of salinomycin and monensin derivatives against Trypanosoma brucei. Parasit Vectors 9:409.

43. Borgstrom B, Huang X, Hegardt C, Oredsson S, Strand D. 2017. Structure-Activity Relationships in Salinomycin: Cytotoxicity and Phenotype Selectivity of Semi-synthetic Derivatives. Chemistry 23:2077-2083.

44. Parry J. 2005. Use of antiviral drug in poultry is blamed for drug resistant strains of avian flu. BMJ 331:10.

45. Perelson AS, Rong L, Hayden FG. 2012. Combination antiviral therapy for influenza: predictions from modeling of human infections. J Infect Dis 205:1642-5.

46. Rosenberg MR, Casarotto MG. 2010. Coexistence of two adamantane binding sites in the influenza A M2 ion channel. Proc Natl Acad Sci U S A 107:13866-71.

47. Tran TT, Kim M, Jang Y, Lee HW, Nguyen HT, Nguyen TN, Park HW, Le Dang Q, Kim JC. 2017. Characterization and mechanisms of anti-influenza virus metabolites isolated

729 from the Vietnamese medicinal plant Polygonum chinense. BMC Complement Altern
730 Med 17:162.
731 48. Jang YJ, Achary R, Lee HW, Lee HJ, Lee CK, Han SB, Jung YS, Kang NS, Kim P, Kim
732 M. 2014. Synthesis and anti-influenza virus activity of 4-oxo- or thioxo-4,5-
733 dihydrofuro[3,4-c]pyridin-3(1H)-ones. Antiviral Res 107:66-75.
734 49. Christodoulopoulos I, Droniou-Bonzom ME, Oldenburg JE, Cannon PM. 2010. Vpu-
735 dependent block to incorporation of GaLV Env into lentiviral vectors. Retrovirology 7:4.
736 50. Jang Y, Lee HW, Shin JS, Go YY, Kim C, Shin D, Malpani Y, Han SB, Jung YS, Kim M.
737 2016. Antiviral activity of KR-23502 targeting nuclear export of influenza B virus
738 ribonucleoproteins. Antiviral Res 134:77-88.
739 51. Vanderlinden E, Vanstreels E, Boons E, ter Veer W, Huckriede A, Daelemans D, Van
740 Lommel A, Roth E, Sztaricskai F, Herczegh P, Naesens L. 2012. Intracytoplasmic
741 trapping of influenza virus by a lipophilic derivative of aglycoristocetin. J Virol 86:9416-
742 31.
743 52. Cotter CR, Jin H, Chen Z. 2014. A single amino acid in the stalk region of the H1N1pdm
744 influenza virus HA protein affects viral fusion, stability and infectivity. PLoS Pathog
745 10:e1003831.
746 53. Vanderlinden E, Goktas F, Cesur Z, Froeyen M, Reed ML, Russell CJ, Cesur N, Naesens
747 L. 2010. Novel inhibitors of influenza virus fusion: structure-activity relationship and
748 interaction with the viral hemagglutinin. J Virol 84:4277-88.
749 54. Fivelman QL, Adagu IS, Warhurst DC. 2004. Modified fixed-ratio isobologram method
750 for studying in vitro interactions between atovaquone and proguanil or

751 dihydroartemisinin against drug-resistant strains of Plasmodium falciparum. Antimicrob
752 Agents Chemother 48:4097-102.
753 55. Forkuo AD, Ansah C, Boadu KM, Boampong JN, Ameyaw EO, Gyan BA, Arku AT,
754 Ofori MF. 2016. Synergistic anti-malarial action of cryptolepine and artemisinins. Malar J
755 15:89.

756

FIGURE LEGENDS

FIG 1. Antiviral activity of salinomycin against influenza viruses. (A) Chemical structure of salinomycin with five ether ring systems (rings A to E in red). The representative carbon positions are numbered in blue. (B) CPE-based antiviral assay. MDCK cells were mock-infected (no virus) or infected with PR8 (A/H1N1 strain), HK (A/H3N2 strain), or Lee (B strain) at an MOI of 0.001. Cells were then exposed to increasing concentrations of salinomycin (ranging from 0.1 to 33.0 μM) for 3 days at 35°C, prior to analysis using an MTT assay. Cell viability ranged from 0% (cells infected with each virus) to 100% (mock-infected cells). Data are expressed as the mean ± standard deviation (SD) of three replicates. n.d., not detected. (C) Western blot analysis. PR8-infected MDCK cells (MOI, 0.001) were treated with 0.1, 1.0, or 10.0 μM salinomycin. OSV-C (0.1 μM) was used as a control. On day 1 p.i., cell lysates were subjected to immunoblot analysis to detect viral proteins, including NP, HA, M1, and M2, together with a cellular protein (β-actin) used as a loading control. (D) Plaque titration. On days 1 and 2 p.i., the amount of infectious viral particles in the culture supernatant was quantified in a plaque assay from three independent samples. The number of particles from virus-infected cells not treated with salinomycin was set at 100%. n.d., not detected.

FIG 2. Effects of salinomycin on the early stages of the influenza virus life cycle. (A) Time of addition experiments. The experimental process is described on the left. MDCK cells were infected with influenza PR8 virus for 1 h at 4°C. After removal of unadsorbed virus, the cells were incubated for an additional 4 h at 35°C. They were inoculated under different conditions,

779 i.e., in the absence or presence of 10 μM salinomycin or EGCG. In parallel, at 1, 2, and 4 h p.i.,
780 the compounds were added to the cell culture medium. At 5 h p.i., the cell monolayers were
781 washed with PBS and overlay medium was added to allow plaque generation. The numbers are
782 expressed as percentages relative to plaque number from the DMSO-treated sample and
783 represent the mean ± SD of triplicate samples. n.d., not detected. (B) Confocal microscopy
784 showing the subcellular distribution of viral NP. MDCK cells were mock-infected (no virus) or
785 infected with PR8 virus at an MOI of 2.5 for 4 h at 37°C in the presence of DMSO, salinomycin,
786 EGCG, or RBV. The viral NP protein was detected using an NP-specific monoclonal antibody
787 and an Alexa Fluor 488-conjugated goat anti-mouse secondary antibody (green). Nuclei were
788 counterstained with DAPI (blue). Original magnification, 400×.
789
790 **FIG 3.** Salinomycin inhibits endosomal acidification. MDCK cells were stimulated with DMSO
791 (mock), salinomycin, bafilomycin A1 (a V-ATPase inhibitor), or chloroquine (an intralysosomal
792 pH neutralizing agent) for 1 h at 35°C. Each sample was then treated with acridine orange (4
793 μg/ml) for 10 min. After excitation at 488 nm, merged images were captured through 590/720
794 nm (red) and 493/560 nm (green) band-pass filters.
795
796 **FIG 4.** Endosomal escape of vRNP is affected by salinomycin. Influenza virus PR8-infected
797 A549 cells (MOI, 10) were treated for 8 h with DMSO (mock) or 10 μM salinomycin in MEM
798 supplemented with 10 μg/ml cycloheximide. Cells were then co-stained for viral NP and the
799 early endosomal marker EEA1 (A) or the late endosomal marker LAMP1 (B). NP protein was
800 visualized with an anti-NP antibody, followed by an Alexa Fluor 633-conjugated secondary

801 antibody (red). EEA1 and LAMP1 were detected using their specific antibodies, followed by an
802 Alexa Fluor-488-conjugated secondary antibody (green). Nuclei were counterstained with DAPI
803 (blue). Original magnification, ×630.
804
805 **FIG 5.** Salinomycin nullifies the proton channel activity of influenza A virus M2. (A) Western
806 blot analysis of influenza viral M2 and MLV p30. VLPs were purified by ultracentrifugation
807 (final volume, 150 μl; 500-fold concentrated) and loaded on a 12% SDS-PAGE gel (2 μl per well)
808 for immunoblotting. Gag-derived p30 capsid (CA) protein was probed with an anti-Gag antibody
809 and a secondary HRP-conjugated goat anti-rat IgG. M2 proteins fused with a His tag were
810 visualized by incubation with an anti-6× His tag antibody and an HRP-conjugated goat anti-
811 mouse antibody. (B) Real-time proton channel assay. Channel activity of PR8M2-S- or PR8M2-
812 R-combined VLPs was measured at 6 s intervals for 5 min in the presence of 100 μM
813 salinomycin or AMT after addition of 150 mM MES (pH 4.5). Null and FCCP-treated VLPs
814 were used as controls. Values represent the average of three independent experiments. (C)
815 Inhibition of M2 channel activity by salinomycin at the experimental end point (5 min). The
816 values represent the mean ± S.D. Statistical analysis was performed using a two-tailed student's
817 *t*-test. ***$p < 0.001$, ****$p < 0.0001$ compared with the DMSO control. (D) Real-time proton
818 channel assay with LeeM2-combined VLPs. Activity was measured at the same time interval and
819 the same condition mentioned in (*B*).
820
821 **FIG 6.** Membrane fusion of cells infected with PR8. (A) Vero E6 cells were infected with PR8 at
822 an MOI of 0.5 at 37°C. At 16 h p.i., cells were preincubated with TPCK-trypsin (5 μg/ml)

823 together with DMSO, 2 μM salinomycin or 0.5 μg/ml anti-HA2 antibody. Cellular membrane
824 fusion was initiated by exposing samples to the indicated conditions (pH 7.0 or 5.6). After
825 staining with Giemsa, fixed cells were visualized by microscopy. Original magnification, ×200.
826 (B) The relative number of nuclei in syncytia was counted from 16 representative images per
827 sample at pH 5.6. Statistical significance was analyzed by comparing differences between the
828 DMSO-treated group and the compound- or antibody-treated groups. ****, $P < 0.0001$.
829
830 **FIG 7.** Isobolograms showing the interaction between salinomycin and OSV-C against wild-type
831 PR8 virus (A and B) and rgPR8(H275Y) mutant strain (C and D). The numbers on the axes
832 represent normalized FIC_{50}s. The sums of both FIC_{50} values (ΣFIC_{50}s) of fixed-ratio interaction
833 and their mean values were quantified (B and D). Interactions were classified as synergistic with
834 ΣFIC_{50}s of <0.8.
835
836 **FIG 8.** *In vivo* antiviral activity of salinomycin in combination with OSV-P against maPR8. (A)
837 Schematic presentation of the antiviral study in a mouse model. Mice were inoculated
838 intranasally with five MLD_{50} doses of mouse-adapted influenza virus PR8 (red arrow). Antivirals
839 were administered orally, once 4 h prior to infection and once 4 h after, and then twice daily for
840 further 5 days (black arrows). Groups of five mice were treated with OSV-P (0.1 mg/kg or 10
841 mg/kg) or salinomycin (10 mg/kg) alone or with a combination of the two (0.1 mg/kg OSV-P and
842 10 mg/kg salinomycin). Body weight changes (B) and mortality (C) were monitored from days 0
843 to 14. Statistical analysis was done using a two-tailed student's *t*-test relative to the OSV-P (0.1
844 mg/kg) group. **, $p < 0.01$; ****, $p < 0.0001$.

845

846 **FIG 9.** *In vivo* antiviral activity of salinomycin in combination with OSV-P against
847 rgK/09Δ(H275Y). Experimental scheme was identical with that of Fig. 8 with minor
848 modifications of OSV-P doses. Groups of five mice were challenged with five MLD_{50} doses of
849 the mouse-adapted OSV-resistant 2009 pandemic strain and treated with OSV-P (10 mg/kg or
850 100 mg/kg) alone or in the presence of salinomycin (10 mg/kg). Body weight changes (A) and
851 mortality (B) were monitored from days 0 to 14. Statistical analysis was performed using a two-
852 tailed student's *t*-test relative to the OSV-P (100 mg/kg) group. *, $p < 0.05$; **, $p < 0.01$; **** p
853 < 0.0001.

TABLE 1. Cytopathic effect-based antiviral assay of selected hit compounds

Compound	CC_{50} (μM)[a] in MDCK cells	EC_{50} (μM)[b] against influenza virus (S.I.[c])		
		PR8[d]	HK[e]	Lee[f]
Atovaquone	>100.0	2.4 ± 0.2 (>41.7)	2.1 ± 0.1 (>47.6)	2.0 ± 0.1 (>50.0)
Evans Blue	>100.0	10.6 ±1.9 (>9.4)	5.4 ± 0.5 (>18.5)	1.5 ± 0.2 (>66.7)
Salinomycin	35.6	0.7 ± 0.1 (48.3)	0.4 ± 0.1 (84.5)	0.8 ± 0.1 (42.3)
AMT[g]	>100.0	>100.0 (n.d.)	0.9 ± 0.2 (>111.1)	>100.0 (n.d.)
RBV[h]	>100.0	18.8 ± 1.8 (>5.3)	12.8 ± 3.2 (>7.8)	13.5 ± 0.5 (>7.4)
OSV-C[i]	>100.0	0.02 ± 0.01 (>5,000)	<0.005 (>20,000)	0.13 ± 0.03 (>769)

[a]Concentration at which cell viability was reduced by 50%;[b]concentration required to improve viability of influenza virus-infected MDCK cells by 50%; [c]selectivity index (ratio of CC_{50}/EC_{50}); [d]A/Puerto Rico/8/34 (H1N1); [e]A/Hong Kong/8/68 (H3N2); [f]B/Lee/40; [g]amantadine hydrochloride; [h]ribavirin; [i]oseltamivir carboxylate.

TABLE 2. Antiviral activity of salinomycin against influenza A/H1N1 strains

Compound	EC_{50} (μM)[a] against influenza A/H1N1 viruses (S.I.[b])						
	A/Brisbane /59/2007	**A/California /7/2009**	**A/Korea /01/2009**	**rgA/Korea /09/2009Δ53-60(H275Y)[c]**	**A/Korea /2785/2009[d]**	**rgA/Puerto Rico /8/1934(H275Y)[e]**	**A/Taiwan /1/1986**
Salinomycin	1.4 ± 0.3 (41.6)	1.9 ± 0.2 (30.3)	1.2 ± 0.0 (48.8)	1.1 ± 0.2 (53.4)	1.7 ± 0.0 (34.0)	0.7 ± 0.1 (86.3)	3.5 ± 0.1 (16.3)
AMT[f]	0.1 ± 0.0 (>90.9)	>100.0 (N.D.)	100.0 (N.D.)	100.0 (N.D.)	100.0 (N.D.)	100.0 (N.D.)	10.5 ± 2.6 (>9.6)
RBV[g]	28.2 ± 6.9 (>3.6)	19.3 ± 0.3 (>5.2)	13.1 ± 2.0 (>7.6)	6.5 ± 2.5 (>15.5)	38.7 ± 4.5 (>2.6)	24.6 ± 0.2 (>4.1)	50.2 ± 1.9 (>2.0)
OSV-C[h]	0.14 ± 0.02 (>740.7)	0.19 ± 0.06 (>526.3)	< 0.005 (>20,000)	4.45 ± 1.97 (>22.5)	2.95 ± 0.55 (>33.9)	1.41 ± 0.03 (>70.9)	0.99 ± 0.21 (>101.5)

[a]Concentration required to improve viability of influenza virus-infected MDCK cells by 50%; [b]selectivity index calculated from the ratio of CC_{50}, which is recorded in Table, to EC_{50}; [c]mouse-adapted, OSV-resistant strain generated by reverse genetics to have a truncation between amino acids 53 and 60 and a point mutation H275Y in NA of rgA/Korea/09/2009Δ53-60; [d]OSV-resistant strain isolated from a Korean patient; [e]OSV-resistant strain generated by reverse genetics to have the H275Y mutation in NA of PR8; [f]amantadine hydrochloride; [g]ribavirin; [h]oseltamivir carboxylate.

TABLE 3. Antiviral activity of salinomycin against influenza A/H3N2, A/H3N8 and A/H9N2 strains

Compound	EC_{50} (μM)[a] against influenza A/H3N2 viruses (S.I.[b])				EC_{50} (μM) against avian influenza viruses (S.I.)	
	A/Brisbane /10/2007	A/Perth /16/2009	A/Seoul /11/1988	A/Victoria /361/2011-like	A/duck/Korea /GJ79/2007 (H3N8)[c]	A/chicken/Korea /MS96/1996 (H9N2)[d]
Salinomycin	2.5 ± 0.1 (22.4)	2.6 ± 0.1 (21.6)	1.3 ± 0.4 (43.2)	1.7 ± 0.3 (34.0)	1.6 ± 0.5 (36.2)	4.2 ± 0.1 (13.5)
AMT[e]	>100.0 (N.D.)	>100.0 (N.D.)	0.1 ± 0.0 (> 1,000)	>100.0 (N.D.)	0.5 ± 0.1 (> 200.0)	0.6 ± 0.3 (> 181.8)
RBV[f]	6.8 ± 0.8 (>14.7)	53.5 ± 1.0 (>1.9)	12.5 ± 3.5 (>8.0)	17.3 ± 3.0 (>5.8)	18.5 ± 0.7 (>5.4)	76.8 ± 4.7 (>1.3)
OSV-C[g]	0.28 ± 0.10 (>357.1)	0.02 ± 0.01 (>5,714)	0.01 ± 0.00 (>10,000)	< 0.005 (>20,000)	0.01 ± 0.00 (>13,333)	0.27 ± 0.01 (>377.4)

[a]Concentration required to improve viability of influenza virus-infected MDCK cells by 50%; [b]selectivity index calculated from the ratio of CC_{50}, which is recorded in Table, to EC_{50}; [c]an avian influenza virus isolated from a duck; [c]an avian influenza virus isolated from a chicken; [e]amantadine hydrochloride; [f]ribavirin; [g]oseltamivir carboxylate.

TABLE 4. Antiviral activity of salinomycin against influenza B strains

Compound	EC_{50} (μM)[a] against influenza B viruses (S.I.[b])			
	B/Florida /4/2006	**B/Panama /45/1990**	**B/Taiwan /2/1962**	**B/Wisconsin /1/2010-like**
Salinomycin	0.4 ± 0.1 (160.3)	0.9 ± 0.1 (29.5)	2.5 ± 0.1 (22.9)	3.8 ± 0.4 (15.0)
AMT[c]	>100.0 (N.D.)	>100.0 (N.D.)	>100.0 (N.D.)	>100.0 (N.D.)
RBV[d]	6.7 ± 2.7 (>15.0)	14.6 ± 2.2 (>6.8)	16.3 ± 1.1 (>6.2)	8.3 ± 0.1 (>12.0)
OSV-C[e]	0.11 ± 0.04 (>909.1)	0.03 ± 0.01 (>4,000)	0.28 ± 0.04 (>357.1)	0.19 ± 0.01 (>540.5)

[a]Concentration required to improve viability of influenza virus-infected MDCK cells by 50%; [b]selectivity index calculated from the ratio of CC_{50}, which is recorded in Table, to EC_{50}; [c]amantadine hydrochloride; [d]ribavirin; [e]oseltamivir carboxylate.

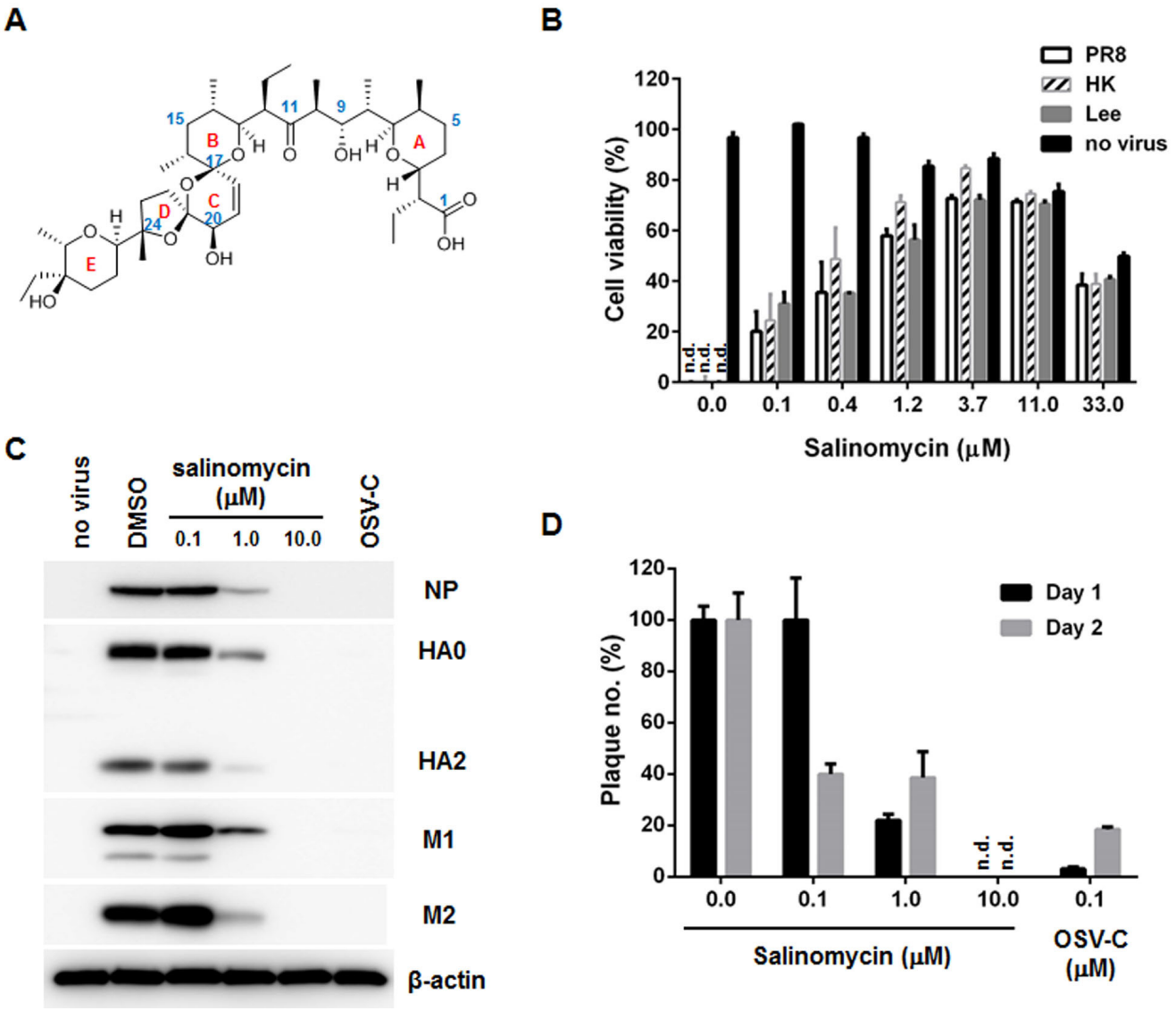

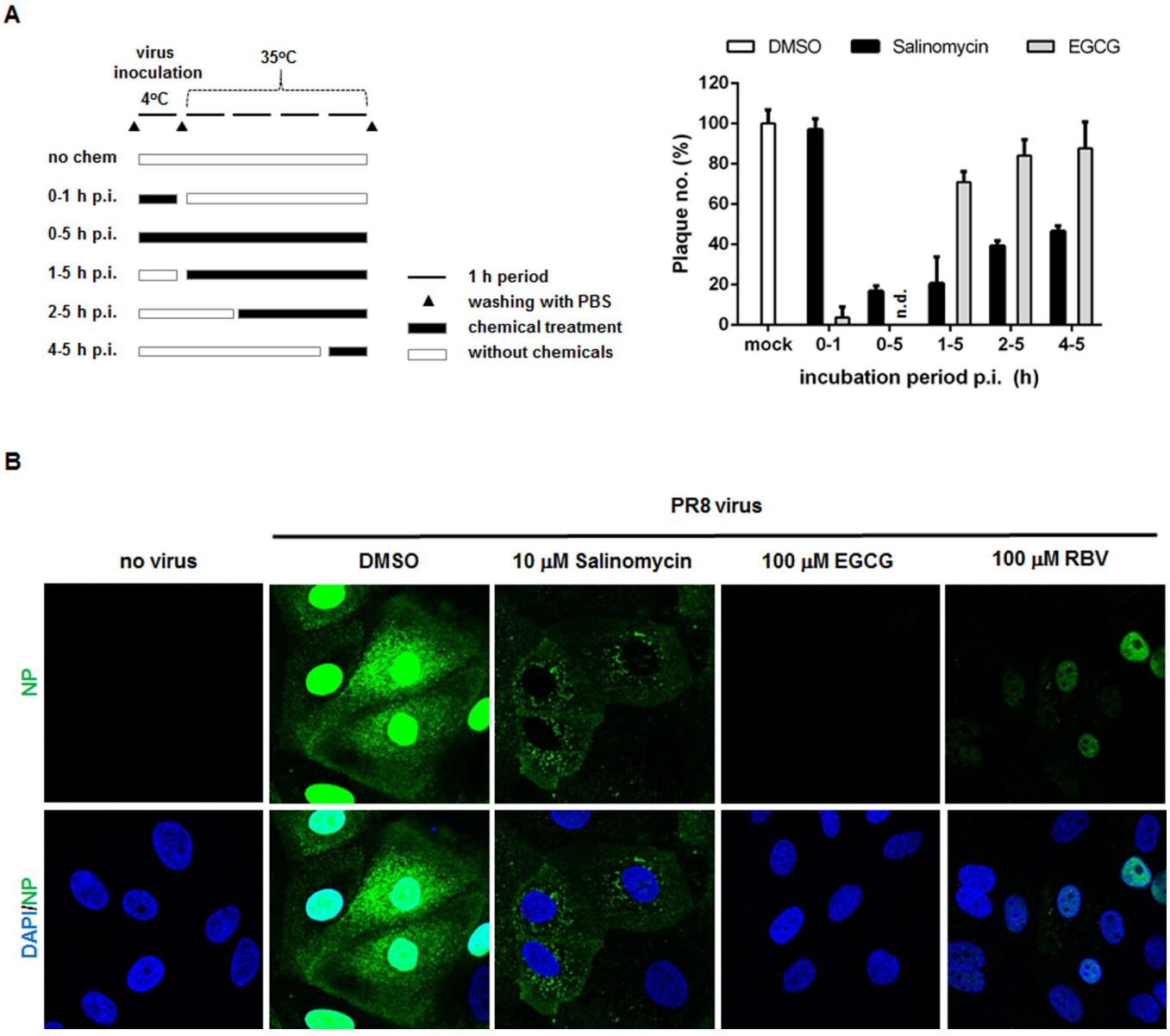

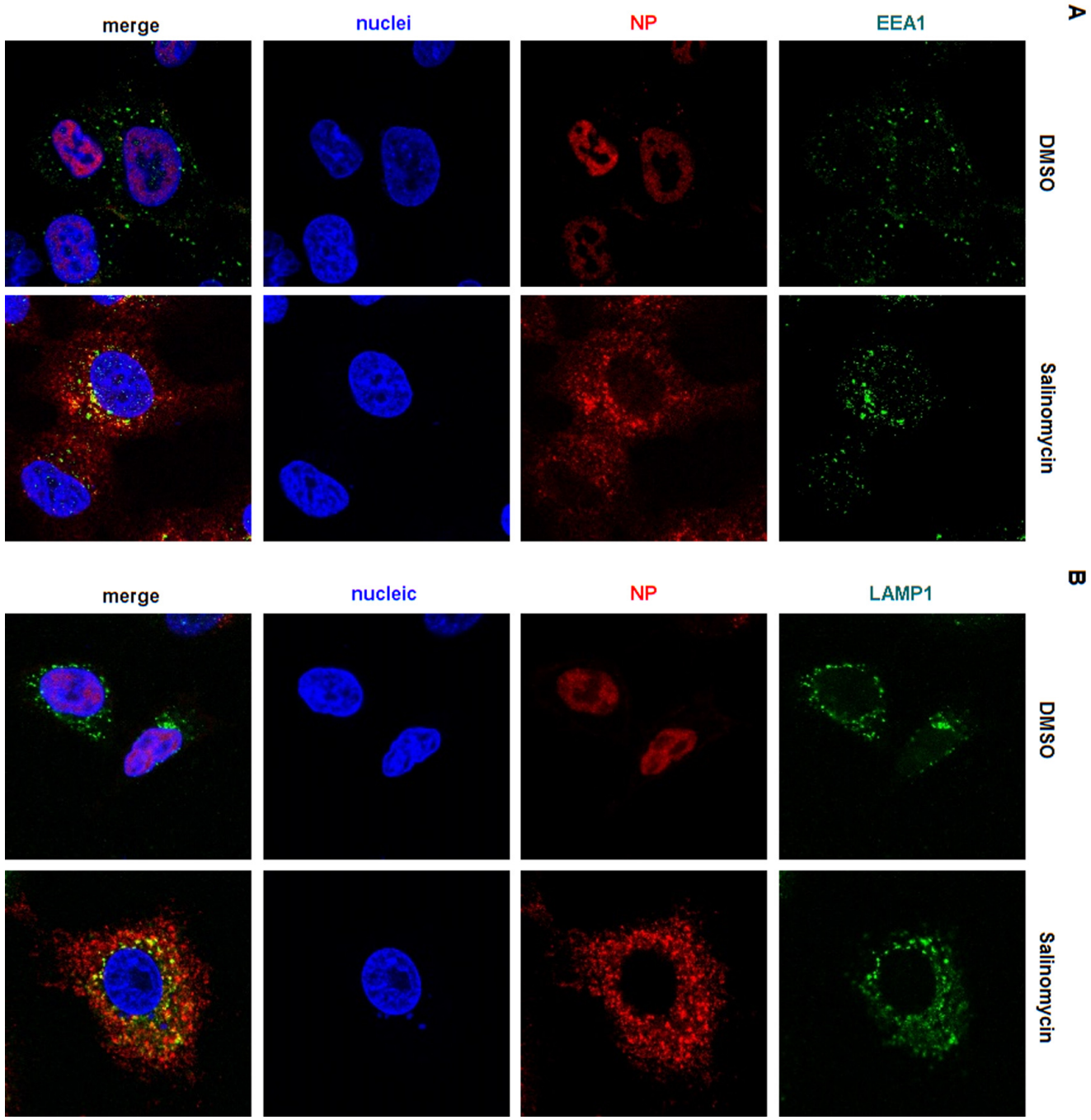

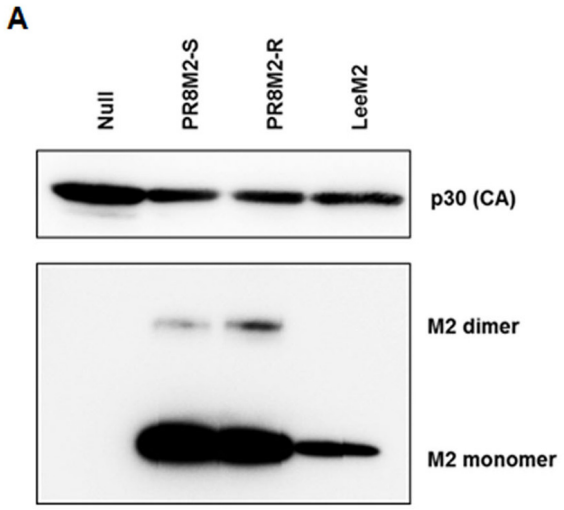

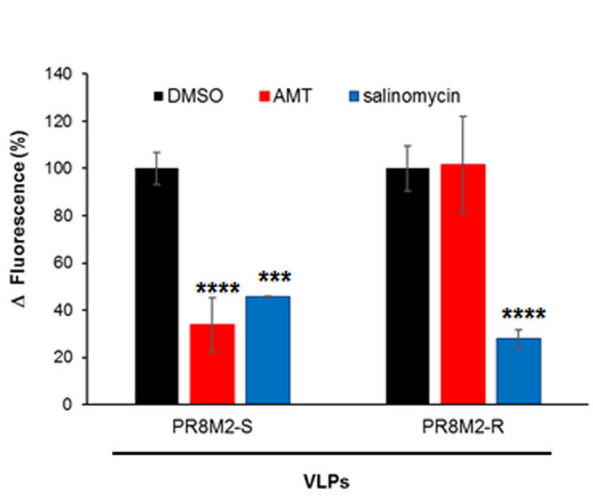

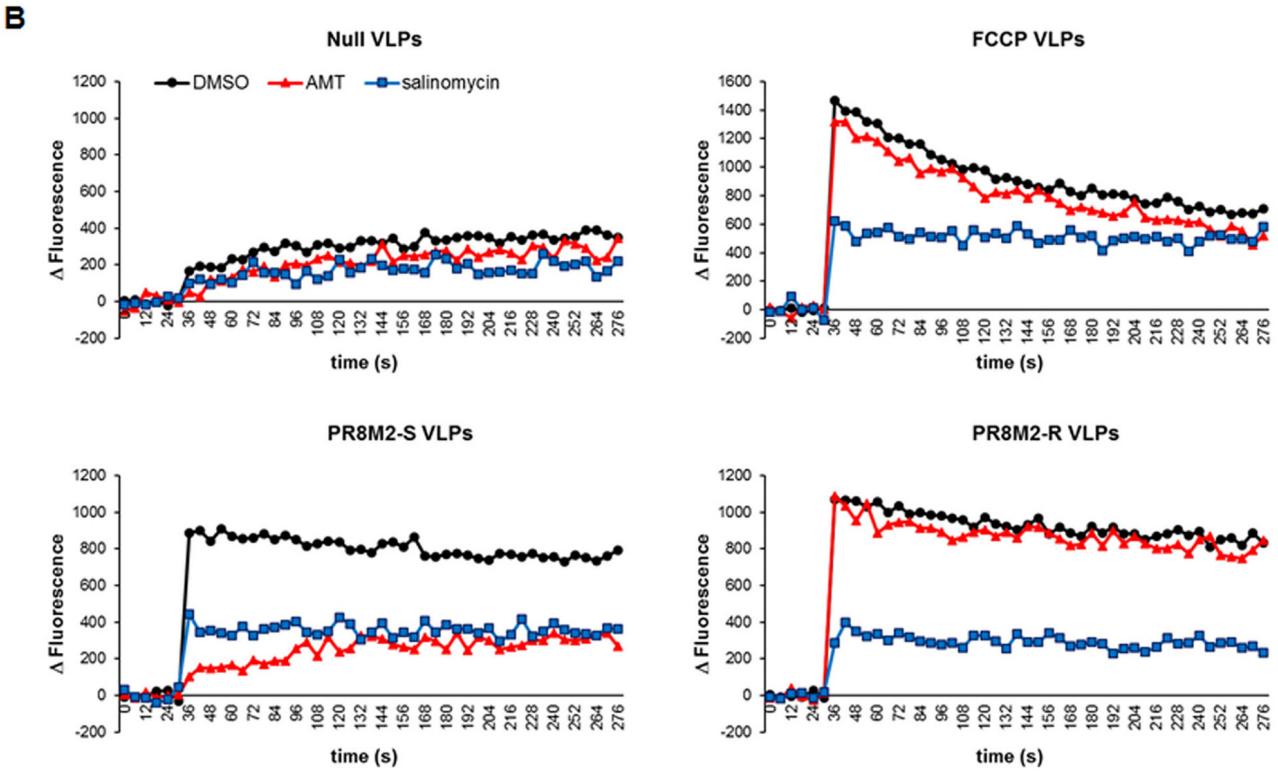

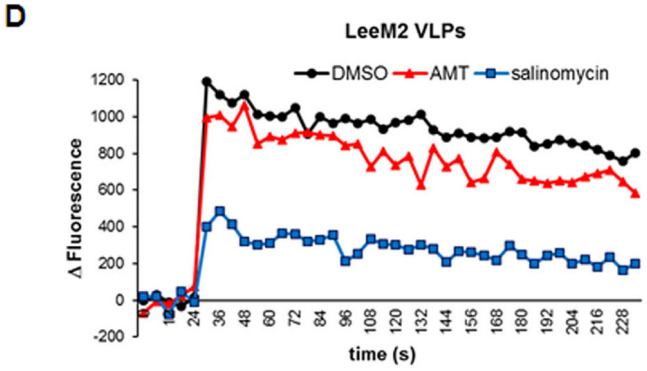

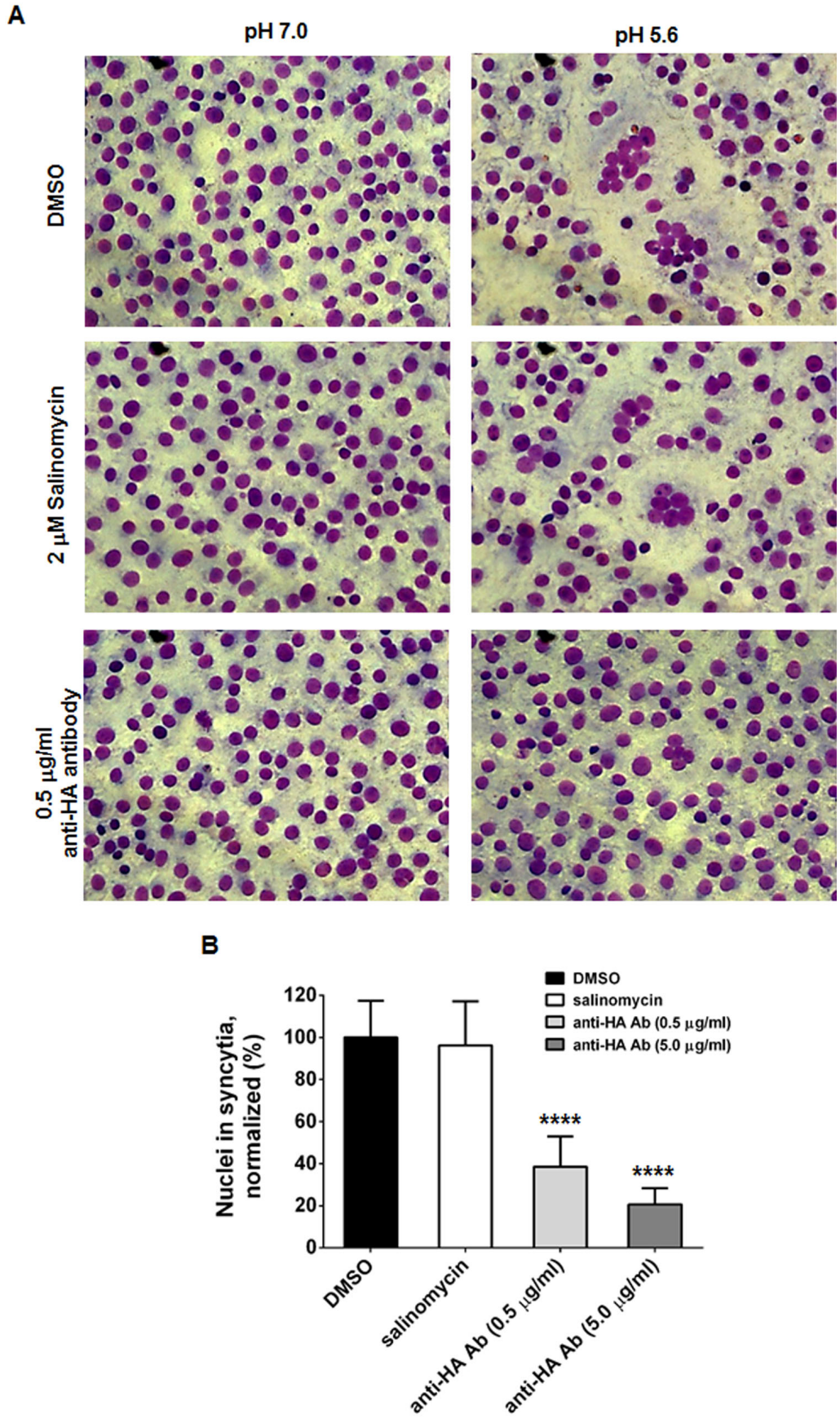

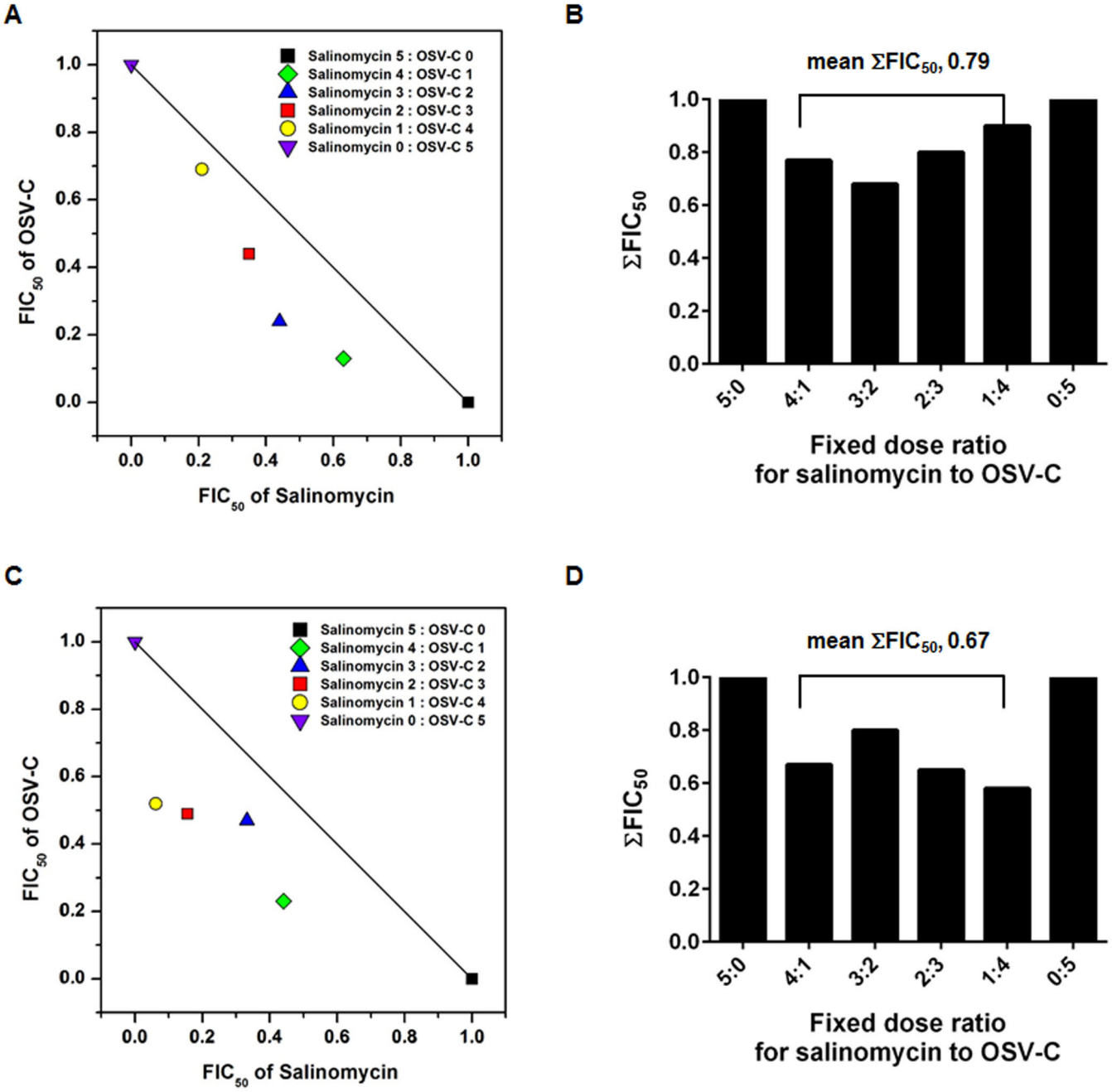

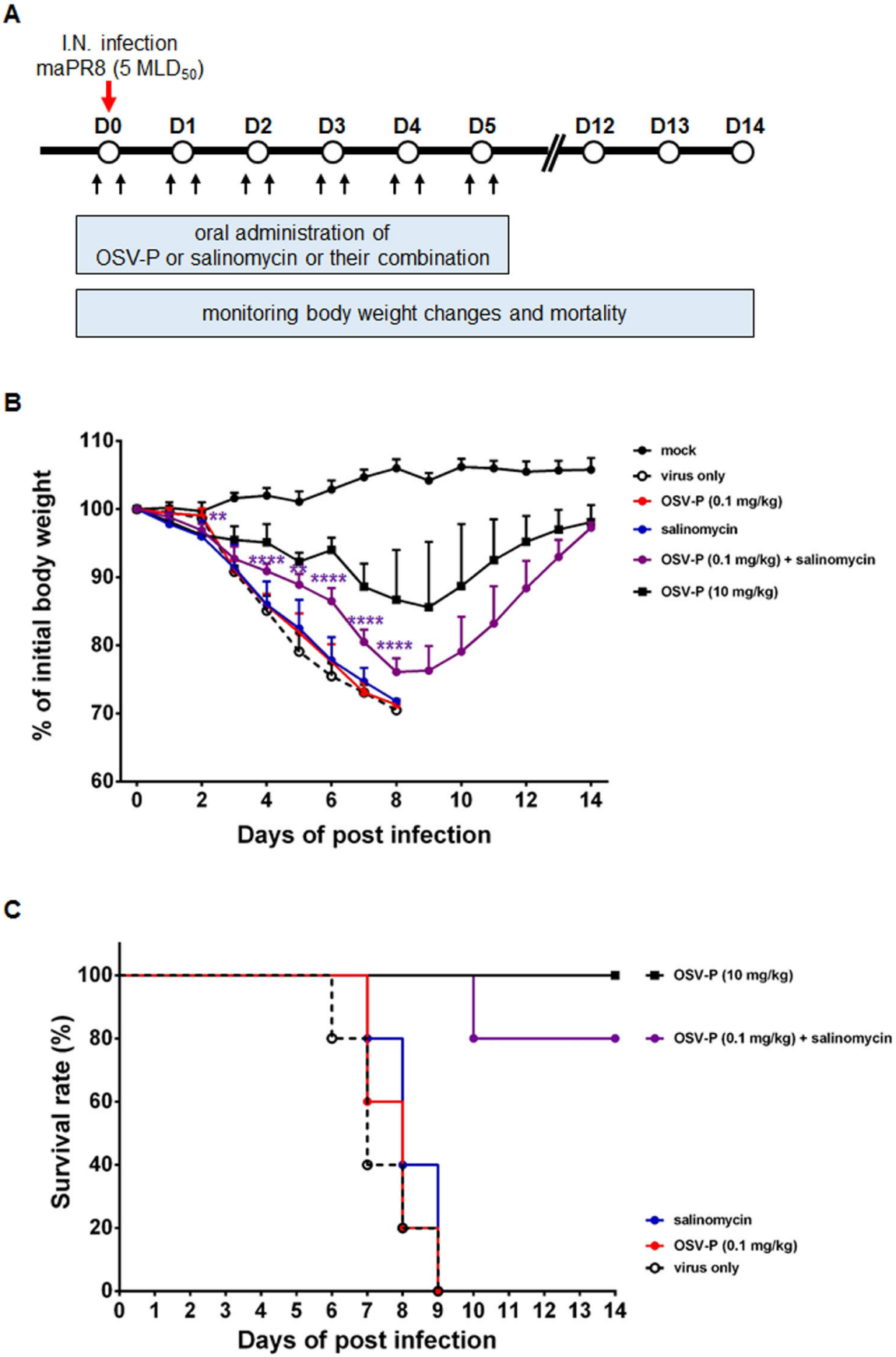

A

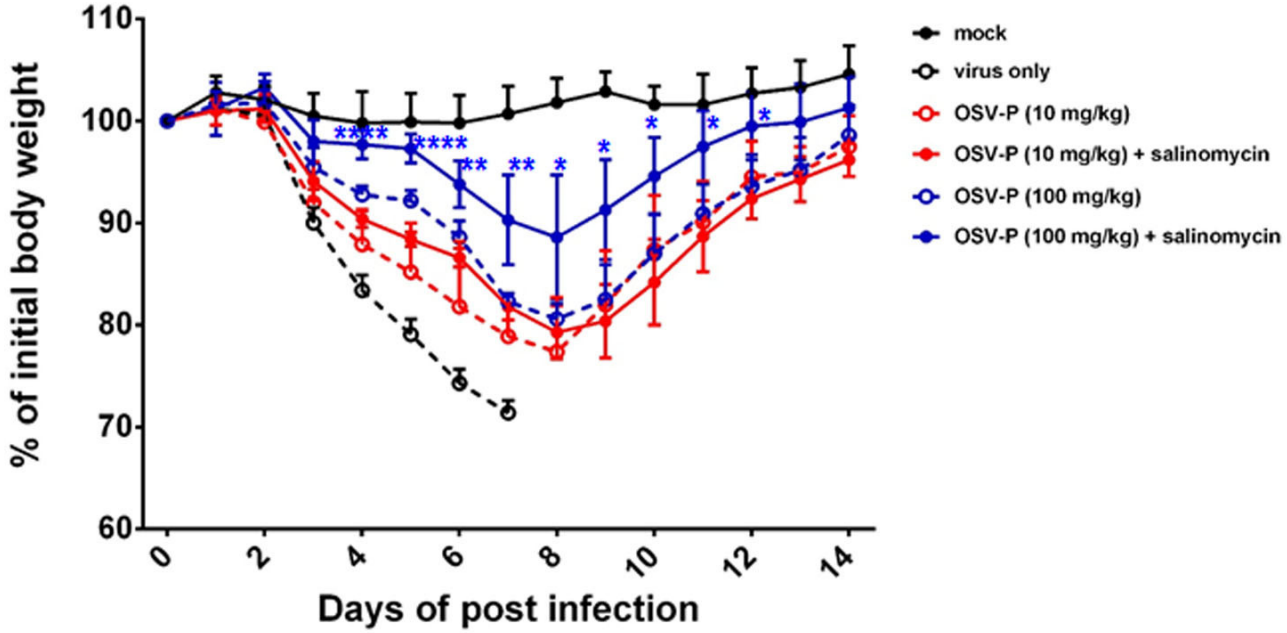

B